Mon. Not. R. astr. Soc. (1984) **209**, 175–208

Steady mildly relativistic thermal plasmas: processes and properties

Roland Svensson★ *European Southern Observatory, Karl-Schwarzschild-Str. 2, D-8046 Garching bei München, West Germany*

Received 1983 December 6; in original form 1983 October 12

Summary. The physical properties of a finite, thermal plasma in pair balance are investigated as a function of the three dimensionless parameters: (i) the temperature θ ($\equiv kT/mc^2$, where m is the electron mass), (ii) the 'proton optical depth' τ_p ($\equiv n_p\sigma_T R$), and (iii) the proton density n_p or radius R. At a dimensionless luminosity l ($\equiv L\sigma_T/Rmc^3 = 3L_{43}/R_{14}$) $\gtrsim 1$ Comptonization of bremsstrahlung and double Compton photons dominates the cooling. A determination of the steady pair density in such a *Wien equilibrium plasma* (WEP) shows the existence of the two pair density branches previously found for optically thin plasmas. Photon–photon absorption modifies the pair annihilation line into a Wien tail.

The $\tau_p-\theta$ parameter space is divided into 11 regions, each characterized by some combination of dominant processes. Pair effects cause part of $\tau_p-\theta$ space to contain three possible states, two of which are pair dominated. For τ_p greater than 10^2–10^5 (depending on n_p) the plasma cloud is necessarily in LTE.

In $l-\theta$ space pair annihilations cannot balance pair productions at $\theta > \theta_{max} \approx 24$ when $l \ll 1$ and at $l > l_{WE}$ when $l \gg 1$ (and $\theta \lesssim 0.4$), where $l_{WE} \approx 4(2\pi)^{1/2}\theta^{5/2}\exp(1/\theta)$ is the luminosity of a pair-dominated WEP. At $\theta \gtrsim 0.1$ the requirement of pair balance can provide a stronger constraint on the luminosity than the pair-free Eddington limit $l_E \approx 10^4 R_s/R$, where R_s is the Schwarzschild radius of the confining mass. At intermediate temperatures, $1/3 \lesssim \theta \lesssim 3$, steady thermal plasmas are possible only for luminosities smaller than L_E by a factor $500(R_s/R)$. The presence of magnetic fields would strengthen these luminosity limits.

Objects observed at MeV energies are discussed with the emphasis on pair effects.

1 Introduction

The formation of mildly relativistic plasmas in compact astrophysical objects such as γ-ray burst sources (Lamb 1982), active galactice nuclei (AGNs; Rees, 1981; Lightman 1982b) and some X-ray binaries is a natural consequence of, e.g. shock velocities greater than 10^4 km s^{-1} (cold matter gets shock heated) or strong enough MeV luminosities

★Present address: NORDITA, Blegdams vej 17, DR-2100 Copenhagen 0, Denmark.

(photon–photon pair production produces a mildly relativistic pair atmosphere – Guilbert, Fabian & Rees 1983). While the physics of hot, though non-relativistic ($\theta \equiv kT/mc^2 \ll 1$) thermal plasmas received much attention in the past (e.g. Felten & Rees 1972; Illarionov & Sunyaev 1972; Lightman 1981 [L81]) it is only recently that progress has been made in the understanding of the properties of relativistic ($\theta > 3$) thermal plasmas (Lightman 1982a [L82]; Svensson 1982 [S82]; Araki & Lightman 1983; Kusunose & Takahara 1983).

Here we attempt to bridge the mildly relativistic temperature range (say $10^{-2} < \theta < 3$) and to explore the properties of a steady, finite, magnetic field-free, thermal plasma cloud uniquely specified by three dimensionless parameters:

$$\theta \equiv kT/mc^2, \qquad \tau_p \equiv n_p \sigma_T R, \qquad n_* \equiv n_p \lambda\!\!\!^{-3}, \tag{1.1}$$

i.e. the dimensionless temperature, the 'proton optical depth' to Thomson scattering, and the dimensionless proton density, respectively (m is the electron mass, n_p the proton density, σ_T the Thomson cross-section, R the cloud radius, and $\lambda\!\!\!^{-}$ the Compton wavelength). The part of parameter space considered is $10^{-4} < \theta < 10^2$ ($10^6\,\mathrm{K} \lesssim T \lesssim 10^{12}\,\mathrm{K}$), any τ_p, and $10^{-24} < n_* < 1$ ($10^7\,\mathrm{cm^{-3}} \lesssim n_p \lesssim 10^{31}\,\mathrm{cm^{-3}}$). The treatment is kept largely analytical by using a very simplified description of the radiative transfer. The assumptions adopted are those of L82 and S82. In particular only internal photon sources are included, and pair balance (pair production equals pair annihilation; pairs do not escape) and photon balance (photon production equals photon escape) are always imposed.

Many properties of a plasma in (local) thermodynamic equilibrium, (L)TE, can be obtained using macroscopic arguments only. In Section 2 we introduce the concept of (necessarily local) Wien equilibrium, WE, and show that macroscopic arguments together with some simple microscopic considerations give a unique luminosity–radius–temperature relationship for a pure electron–positron pair cloud in WE. Microscopic processes receive full attention in Section 3, where the pair balance equation at mildly relativistic temperatures is solved with special emphasis on WE plasmas (WEPs). Comptonization of bremsstrahlung and double Compton photons are the dominant radiation mechanisms, while pairs are produced in photon–photon interactions.

With a solid understanding of the pair balance solutions it is possible in Section 4 to divide the τ_p–θ parameter space into 11 regions, each characterized by some combination of dominant processes. The dependence on n_* is considered separately. It is then a trivial matter to determine the characteristics of a plasma cloud given θ, τ_p, and n_*. The luminosity as a function of θ and τ_p is determined in Section 5 for radii 10^6 cm (γ-ray burst source, black hole X-ray binary) and 10^{14} cm (AGN). The effects of pairs are most easily visualized in a luminosity–temperature diagram in which a large region is shown to be forbidden for thermal plasmas in pair balance. The few objects observed at MeV energies as well as objects observed at X-ray energies are discussed in Section 6 in terms of the luminosity–temperature diagram to determine if pair production occurs in these objects. Finally, in Section 7 some directions for future work are pointed out.

A few appendices contain details of soft photon production (bremsstrahlung, double Compton, three quantum annihilation and radiative pair production) at mildly relativistic temperatures, two-body reaction rates in WEPs, and an approximate treatment of mildly relativistic Comptonization.

2 Equilibrium plasmas – some general aspects

When a plasma is in a thermodynamic equilibrium (TE; the photon chemical potential μ_γ is equal to zero) or in Wien equilibrium (WE; $\mu_\gamma \ll 0$), macroscopic arguments suffice

to determine important properties of the plasma. Of particular interest here are the pair density in a plasma cloud in WE and its luminosity. It is useful to discuss first the corresponding properties of a TE plasma. (Traditionally the terms TE and LTE have been used to describe only the thermodynamic equilibrium situation where $\mu_\gamma = 0$. To avoid confusion we use WE to denote the thermodynamic equilibrium situation where $\mu_\gamma \ll 0$.)

2.1 THERMODYNAMIC EQUILIBRIUM

The relationship between the positron (or pair) density n_+, the electron density n_-, the proton density n_p, and the temperature θ in an ionized hydrogen plasma in TE is discussed in, e.g. Chiu (1968) and Wandel & Yahil (1979). Here we write the relationship in the form

$$n_+ n_- = \lambda\!\!\!^{-}{}^{-6}\, 4\left(\frac{\theta}{2\pi}\right)^3 \exp(-2/\theta)\, g_{\rm TE}(\theta, n_p), \tag{2.1}$$

where the densities are further related through charge conservation

$$n_- = n_+ + n_p. \tag{2.2}$$

Two limiting forms of $g_{\rm TE}$ are of interest. At non-relativistic temperatures $g_{\rm TE} = 1$, while in pure pair plasmas

$$g_{\rm TE}(\theta, n_p = 0) = [1 + 0.3726\theta^{1/2} + 0.4724\theta + 3(2\pi)^{-1/2}\,\zeta(3)\theta^{3/2}]^2 \tag{2.3}$$

to within 2 per cent [$\zeta(3) = 1.202$ is the Riemann zeta function].

As the photon density n_γ in TE is

$$n_\gamma = \lambda\!\!\!^{-}{}^{-3}\,\zeta(3)\,2\pi^{-2}\theta^3, \tag{2.4}$$

we find that the ratio of photons to particles is

$$\frac{n_\gamma^2}{n_+ n_-} = [\zeta(3)]^2\,\frac{8}{\pi}\,\theta^3 \exp(2/\theta)\, g_{\rm TE}^{-1}. \tag{2.5}$$

In a pure pair plasma the photon to pair ratio, n_γ/n_+, increases exponentially towards non-relativistic temperatures ($\theta \ll 1$) as $\zeta(3)\,(8\theta^3/\pi)^{1/2} \exp(1/\theta)$, while for relativistic temperatures ($\theta \gg 1$) the ratio becomes 4/3.

A spherical plasma cloud of radius R and temperature T radiates in LTE a luminosity

$$L_{\rm BB} = 4\pi R^2 \sigma T^4 = 7 \times 10^{44}\, R_{14}^2\, T_5^4 \ {\rm erg\ s^{-1}} \tag{2.6}$$

($R = R_{14}\, 10^{14}$ cm, $T = T_5\, 10^5$ K, σ is the Stefan–Boltzmann constant), which is a function of R and T only. If, however, scatterings dominate the opacity then the luminosity is reduced to (modified black body)

$$L_{\rm MB} \approx 4\pi R^2 \sigma T^4\, \tau_{\rm cs}^{-1}, \tag{2.7}$$

where $\tau_{\rm cs}$ is the frequency averaged Compton scattering optical depth down to the layer where a Planckian radiation field becomes established (or, equivalently, where an incident radiation beam gets absorbed). The modified luminosity depends not only on T and T, but also on the density and on the type of radiation mechanism that dominates.

2.2 WIEN EQUILIBRIUM

As Nature contains processes that do not conserve the sum of particles and photons it follows that no real systems can be in true WE. However WE may be closely approached (local WE) in finite systems if the time-scale for establishing WE is shorter than the time-scales for photon production and photon escape. Contrary to the TE case the *absolute* levels of photons and particles in WE follows only from microscopic considerations. Their *relative* level is, however, given by macroscopic thermodynamic arguments (Svensson 1983)

$$\frac{n_\gamma^2}{n_+ n_-} = \left[\frac{2\theta^2}{K_2(1/\theta)}\right]^2 = \frac{8}{\pi}\theta^3 \exp(2/\theta)\, g_{\rm WE}^{-1}, \tag{2.8}$$

where $K_n(x)$ is the modified Bessel function of the second kind of order n and where the numerically fitted polynomial

$$g_{\rm WE}(\theta) = 1 + 3.7622\theta + 5.1054\theta^2 + \frac{8}{\pi}\theta^3 \tag{2.9}$$

is accurate to 0.06 per cent. At relativistic temperatures $n_\gamma^2/n_+n_- \to 1$. This ratio behaves similarly in both the WE and the TE cases. For example, in a pure pair plasma in WE $n_\gamma/n_+ = (8\theta^3/\pi)^{1/2}\exp(1/\theta)$ for $\theta \ll 1$ and $n_\gamma/n_+ = 1$ for $\theta \gg 1$.

We now show that for a pair-dominated ($n_+ \gg n_{\rm p}$) plasma cloud in WE there exists a unique luminosity–radius–temperature relationship, just as was the case for an LTE-cloud (equation 2.6). The concept of WE necessarily requires that radiation transport is through scatterings, and not through true absorptions and emissions. If the total photon production rate is $\dot{n}_\gamma\ {\rm cm^{-3}\ s^{-1}}$, then the luminosity of a uniform spherical cloud becomes

$$L_{\rm WE} = \frac{4\pi R^3}{3} 3kT\dot{n}_\gamma, \tag{2.10}$$

where $3kT$ is the mean energy of Wien photons. The need to know the microscopic photon generation process is eliminated by using the fact that in steady state the photon generation rate, $\dot{n}_\gamma$, is equal to the diffusive escape rate,

$$\dot{n}_\gamma = n_\gamma t_{\rm esc}^{-1} \approx n_\gamma\left(\xi\frac{R}{c}\tau_{\rm w}\right)^{-1} = n_\gamma\left(\xi\frac{R}{c}\tau_{\rm T} g_\tau\right)^{-1}, \tag{2.11}$$

where $t_{\rm esc}$ is the diffusive escape time for photons, ξ is a geometrical factor ($\approx 1/3$ for a spherical cloud and ≈ 1 for a slab; $\xi = 1/3$ is used in all figures), $\tau_{\rm w}$ is the Wien averaged scattering optical depth (equation B14), $\tau_{\rm T}$ is the Thomson scattering optical depth of the cloud

$$\tau_{\rm T} = (n_+ + n_-)\,\sigma_{\rm T} R, \tag{2.12}$$

and $g_\tau(\theta)$ describes the Klein–Nishina corrections of $\tau_{\rm w}$ (equation B13). Domination of pairs gives $\tau_{\rm T} = 2n_+\sigma_{\rm T}R$. Then $\dot{n}_\gamma \propto (n_\gamma/n_+)R^{-2}$ which is a function of temperature θ (see equation 2.8) and radius R only. The luminosity of a pair-dominated cloud becomes

$$L_{\rm WE} = \frac{mc^3}{\sigma_{\rm T}} R 4(2\pi)^{1/2}\,\theta^{5/2}\exp(1/\theta)(\xi g_\tau g_{\rm WE}^{1/2})^{-1}, \tag{2.13}$$

where the dependence on R follows from $({\rm volume}/t_{\rm esc}) \propto R^3/R^2 \propto R$. Expressing the luminosity as a dimensionless quantity

$$l \equiv \frac{L}{R}\frac{\sigma_{\rm T}}{mc^3} = 2.7\, L_{43}/R_{14} \tag{2.14}$$

($L = L_{43}\, 10^{43}$ erg s^{-1}), we find that the function $l_{WE} = L_{WE}\sigma_T/(mc^3R)$ depends on temperature only, has a minimum value of $20/\xi \approx 60$ (if $\xi \approx 1/3$) at $\theta \approx 0.37$ ($T \approx 2.2 \times 10^9$ K), and increases exponentially towards smaller temperatures. For sizes (from soft X-ray time variability) characteristic of AGNs we have the minimum WE-luminosity $L_{WE} = 2.2 \times 10^{44}\, R_{14}$ erg s^{-1}, which, remarkably enough, is of the same order of magnitude as observed luminosities.

As the luminosity L_{WE} increases rapidly with *decreasing* temperatures ($dL/d\theta < 0$) it necessarily becomes equal to the luminosity L_{MB} (not L_{BB} as scattering opacity dominates) at some temperature θ_t. Here the plasma cloud becomes effectively thick (i.e. the radiation field in the centre becomes Planckian) and the scattering depth τ_{cs} in equation (2.7) approximately equals $\xi\tau_w$. The condition determining the transition from an effectively thin to an effectively thick cloud is given by

$$R = (\xi\tau_w)\frac{\lambda\!\!\!^{-3}}{\sigma_T}\frac{60}{\pi^3}(2\pi)^{1/2}\,\theta_t^{-3/2}\exp(1/\theta_t)(\xi g_\tau g_{WE}^{1/2})^{-1}. \tag{2.15}$$

Although $\xi\tau_w$ is only known once the microscopic processes have been specified it is clear from equation (2.15) that the 'transition' temperature θ_t is only weakly (logarithmic) dependent of the value of $\xi\tau_w$. For $R = 10^{14}$ cm the transition temperature becomes $\theta_t = 0.026$, 0.029 for $\xi\tau_w = 1$, 100, respectively. Once effectively thick the cloud luminosity increases with *increasing* temperature ($dL/d\theta > 0$).

Thus in a pair-dominated WEP experiencing an ever increasing heating rate at termperatures $\theta < 0.37$ the temperature first decreases, while $n_\gamma/n_+ \gg 1$ increases as $(8\theta^3/\pi)^{1/2}\exp(1/\theta)$. At θ_t the cloud centre reaches LTE, which causes the temperature to increase, while n_γ/n_+ decreases initially as $1.2\,(8\theta^3/\pi)^{1/2}\exp(1/\theta)$ until it approaches its relativistic TE value of 4/3. The ratio n_γ/n_+ thus achieves its maximum value at θ_t.

In an effectively thin cloud not dominated by pairs the luminosity normally *increases* with temperature. Hence, $dL/d\theta$ should also change sign at some temperature θ_c close to the temperature where a cloud becomes pair-dominated if this transition occurs in WE and if the temperature θ is less than 0.37. We conclude that for temperatures between θ_t and θ_c there should exist three possible states of the plasma cloud, one pair-free state and two pair-dominated states (one in WE and the other in TE).

Although much information about pair plasmas in WE is obtainable from mainly thermodynamic considerations, it is only by treating the microphyscis that we can make further progress in understanding when plasmas are pair-dominated, what the dominant processes are, and when WE is established.

3 Pair balance in mildly relativistic plasmas

3.1 THE GENERAL CASE

Instead of solving the full radiative transfer problem coupled with pair balance in a spherical cloud we make some considerable simplifications leading to the necessity of solving at most three non-linear algebraic equations, thus making a full exploration of parameter space (θ, τ_p, n_*) easy to perform. More precisely, only the conditions at some average point (e.g. the centre) of the cloud are studied. The steady pair density is obtained by solving the pair balance equation

$$(\dot{n}_+)_{\gamma\gamma} + (\dot{n}_+)_{\gamma e} + (\dot{n}_+)_{\gamma p} + (\dot{n}_+)_{ee} + (\dot{n}_+)_{ep} - \dot{n}_A = 0, \tag{3.1}$$

where the first five terms represent the pair production rates [cm^{-3} s^{-1}] in $\gamma\gamma$, γe, γp, ee and ep collisions, respectively, and where $\dot{n}_A$ is the pair annihilation rate. The

spectral density of photons enters in the first three terms requiring a solution of the radiative transfer problem.

The photon generating processes in a magnetic-field free plasma are listed in Table 1 in S82. When optical depths are small only bremsstrahlung ($ep \rightarrow ep\gamma$ or $ee \rightarrow ee\gamma$) is important. If, however, Comptonization of soft photons occurs, then double Compton scattering ($e\gamma \rightarrow e\gamma\gamma$), three quantum annihilation ($e^+e^- \rightarrow \gamma\gamma\gamma$), and radiative pair production ($\gamma\gamma \rightarrow e^+e^-\gamma$) (all of which exhibit infrared divergencies) may compete with bremsstrahlung. All these processes have a spectral emissivity, $\dot{n}(x, \theta)dx$ cm^{-3} s^{-1}, of photons at dimensionless energy x (in units of mc^2) that at soft energies ($x \ll \theta$) are of the form

$$\dot{n}(x, \theta)\, dx = n_1 n_2 c r_e^2 \alpha \frac{dx}{x} F(x, \theta), \tag{3.2}$$

where n_1 and n_2 are densities (see Fig. 1 for details), α is the fine structure constant, r_e is the classical electron radius, and $F(x, \theta)$ is a temperature-dependent function given or determined in Appendix A and shown in Fig. 1 (only for bremsstrahlung is there a weak logarithmic dependence of F on x; x is chosen to be 10^{-6} in Fig. 1). It is immediately clear that three quantum annihilation is negligible relative to e^+e^- bremsstrahlung, both emissivities being proportional to n_+n_-. Large radiative pair production requires large photon densities, which in turn implies large scattering depths and the establishment of WE. In WE, however, radiative pair production is no more important than three quantum annihilation (equation A20, and the RPP and 3QA curves in Fig. 1). Double Compton scattering, being dependent on the photon density, may dominate over bremsstrahlung in WE. In pair-dominated WE this occurs for $\theta \lesssim 0.1$ (using the DCWE curve in Fig. 1), as n_γ/n_+ reaches exponentially large values towards smaller θ (equation 2.8). The radiation processes of interest are thus bremsstrahlung and double Compton.

Assuming that the Compton scattering opacity dominates at pair producing photon energies the radiative transfer problem is simply treated using escape times and by assuming an isotropic photon distribution. When the scattering optical depth is small ($\tau_{cs} < 1$) the photon spectral density, $n_B(x)$ cm^{-3}, is determined by

$$\dot{n}_{ep}(x) + \dot{n}_{ee}(x) + \dot{n}_{+-}(x) - t_{esc}^{-1} n_B(x) = 0, \tag{3.3}$$

where the bremsstrahlung emissivities are discussed in S82 and where $t_{esc} = R/c$. The radiation field $n_B(x)$ can be solved for explicitly and inserted into the rates in the pair balance equation. The temperature-dependent part of these rates is obtained by finding analytical fits to the results of numerical integrations (see S82 for a detailed discussion of the rates in equation 3.1). The pair balance equation then reduces to a polynomial equation for the pair density variable

$$z \equiv n_+/n_p \tag{3.4}$$

with coefficients dependent on the parameters θ and τ_p (see L82 and S82), and the solving of a single equation determines $z(\theta, \tau_p)$.

When Comptonization is important the spectral density of equation (3.3) is replaced by the sum of a Wien spectral density

$$n_w(x)\, dx = n_\gamma \tfrac{1}{2}(x/\theta)^2 \exp(-x/\theta)\, dx/\theta \tag{3.5}$$

and a 'flat' part which, when bremsstrahlung dominates, is approximately given by

$$n_F(x)\, dx = \frac{\theta}{\bar{\lambda}^3} \frac{x_m^2}{\pi^2} \frac{dx}{x} \exp(-x/\theta) \left(\frac{1}{\ln \theta/x_m} + \frac{y_1}{1+y_1} \right), \tag{3.6}$$

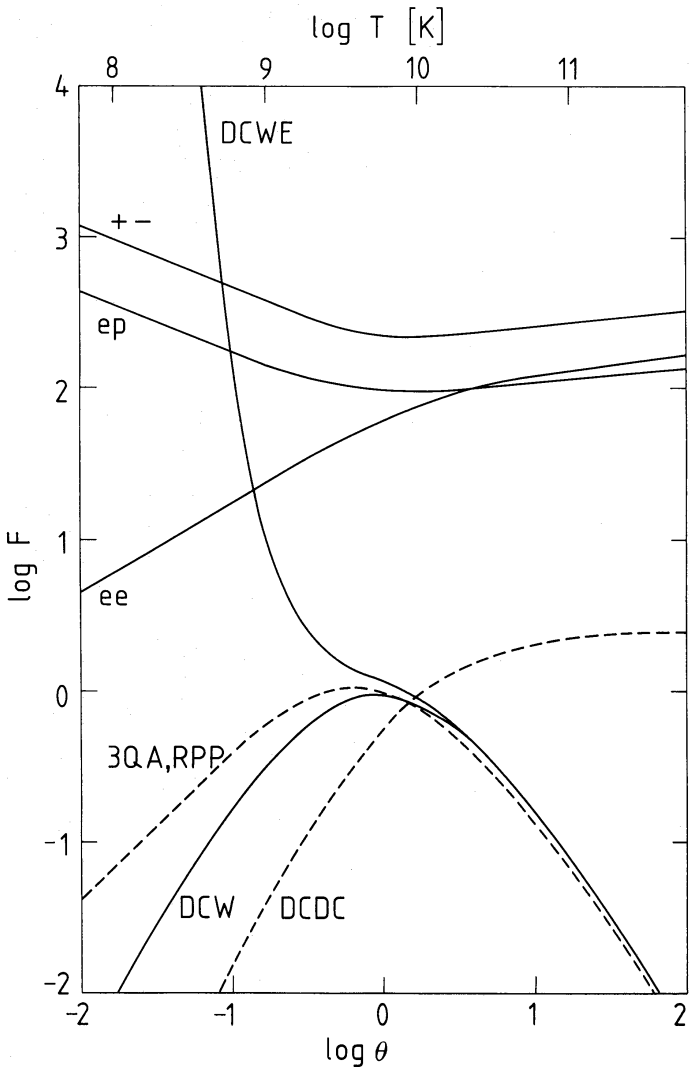

Figure 1. The dimensionless emissivity $F(x = 10^{-6}, \theta) \equiv \dot{n}(x, \theta)\, x/(n_1 n_2 c r_e^2 \alpha)$ in the soft photon limit ($x \ll \theta$). The process and $n_1 n_2$ for each curve are $+-$: e^+e^- bremsstrahlung, $n_+ n_-$; ep: ep bremsstrahlung, $(n_+ + n_-) n_p$; ee: $e^{\pm}e^{\pm}$ bremsstrahlung, $n_\pm^2 + n_\pm^2$; DCW: double Compton from a Wien distribution, $n_\gamma(n_+ + n_-)$; DCDC: double Compton from a double Compton distribution, $N_\gamma(n_+ + n_-)$; DCWE: double Compton in pair-dominated Wien equilibrium, $n_\pm^2$; 3QA: three quantum annihilation, $n_+ n_-$; RPP: radiative pair production in Wien equilibrium, $n_+ n_-$, respectively. $F(x, \theta)$ depends on x (logarithmically) for bremsstrahlung only. See Appendix A for definition of N_γ and further details.

where x_m (determined by equation D2) is the photon energy below which the local spectrum is Planckian. The last factor of equation (3.6) is designed to be of order unity when Comptonization is saturated ($y_1 \gg 1$; for y_1, see Appendix C) and to make the 'flat' spectrum approximately coincident with the bremsstrahlung spectrum near $x \approx \theta$ when Comptonization is unimportant. The pair-production rates for the spectral shapes of equations (3.5) and (3.6) are evaluated in Appendix B. The photon density, n_γ, of the Wien peak (equation 3.5) is determined by solving

$$f_B \dot{n}_\gamma^B + f_{DC} \dot{n}_\gamma^{DC} - t_{esc}^{-1} n_\gamma = 0, \tag{3.7}$$

where $\dot{n}_\gamma^B$ and $\dot{n}_\gamma^{DC}$ are the total generation rates of bremsstrahlung photons and double Compton photons, respectively, with energies larger than x_m (Appendix A5), where f_B and f_{DC} are the fractions of these photons that scatter into the Wien peak before escaping

(Appendix C), and where $t_{esc} = (R/c)(1 + \xi\tau_w)$ with the Wien averaged scattering optical depth τ_w being given by equation (B14).

To bridge the transition from the optically thin case to the Comptonized case the following interactions between the three types of radiation fields were found to be important in the photon–photon pair production term in equation (3.1): $n_B(x) \cdot n_B(x)$ (fig. 3 in S82), $n_w(x) \cdot n_w(x)$ (equation B6), and $n_F(x) \cdot n_w(x)$ (equation B7). Then to determine completely the properties of a plasma cloud in the general case, three non-linear algebraic equations (equations 3.1, 3.7 and D2) must be solved for z, x_m, and the dimensionless photon density

$$r \equiv n_\gamma / n_p \tag{3.8}$$

in terms of the three parameters θ, τ_p, and n_*. The solutions for z as a function of θ for $10^{-5} < \tau_p < 10^2$ and for $n_* = 10^{-20}$ ($n_p \approx 10^{11}$ cm^{-3}) are shown in Fig. 2. For a given τ_p there are two solution branches, one high-z and one low-z, that merge at the temperature $\theta_c(\tau_p, n_*)$. For $\theta > \theta_c(\tau_p, n_*)$ pair productions occur faster than pair annihilations and pair balance does not occur. The temperature θ_c is a decreasing function of τ_p and depends only weakly on n_*. Equivalently, for every θ in an effectively thin plasma there is a maximum possible scattering optical depth $\tau_p^{max}(\theta, n_*)$, which is shown in Fig. 3 (the rightmost thick solid curve) for $n_* = 10^{-10}$. The high-z branches in Fig. 2 join the dashed curve (representing the pair density in TE) at $\theta_t(\tau_p, n_*)$. Here the plasma cloud becomes effectively thick and larger values of z only occur in TE at larger temperatures. Equivalently, there exists a minimum possible scattering optical depth $\tau_p^{min}(\theta, n_*)$ for the high-z state in an effectively thin plasma (shown in Fig. 3 by the leftmost thick solid curve). The

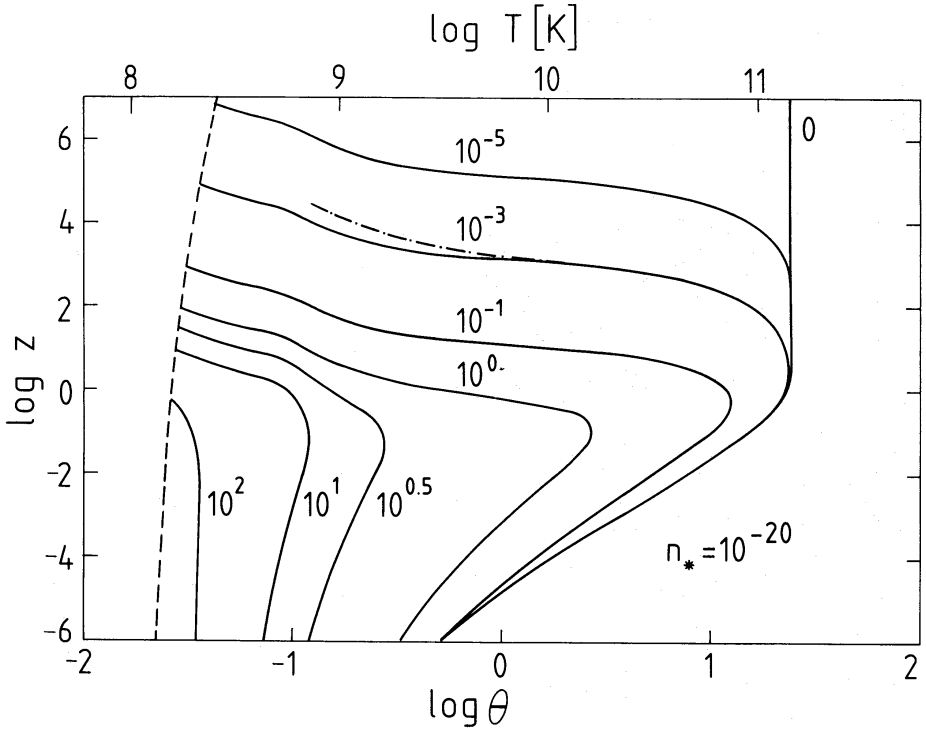

Figure 2. The dimensionless pair density $z \equiv n_+/n_p$ in an effectively thin plasma in pair balance is shown for $n_* = 10^{-20}$ by the solid curves. Each curve is labelled by its value of the 'proton' optical depth $\tau_p = n_p \sigma_T R$. The dashed curve shows the pair density in an effectively thick plasma (i.e. in thermodynamic equilibrium) with $n_* = 10^{-20}$. The dashed-dotted curve shows the pair density for $\tau_p = 10^{-3}$ and $n_* = 10^{-10}$.

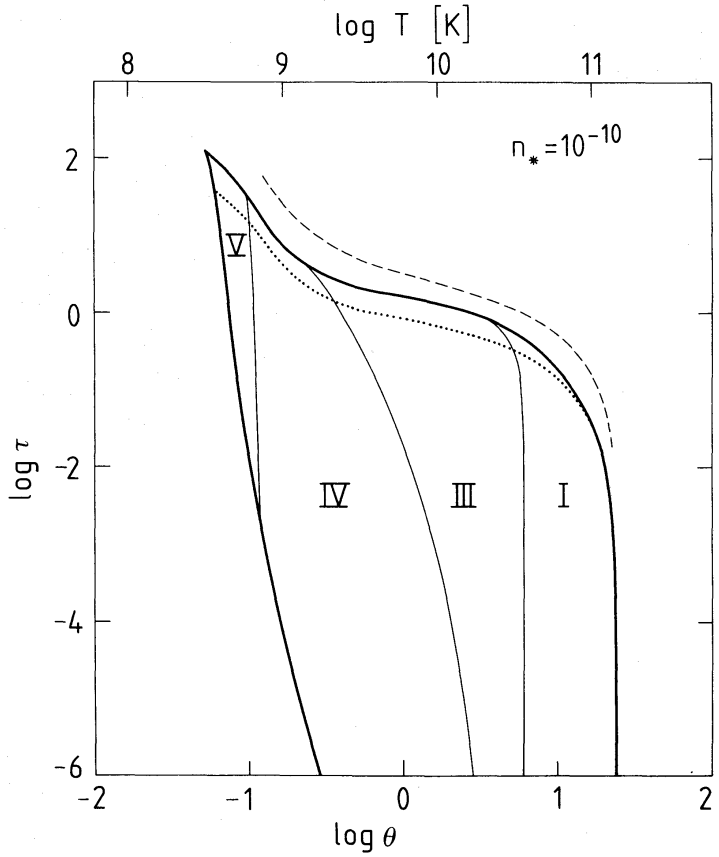

Figure 3. The τ_p–θ parameter space of the high-z solutions in an effectively thin plasma is bounded by the thick solid curves. For given τ_p and n_* there exist a maximum temperature, $\theta_c(\tau_p, n_*)$, and a minimum temperature, $\theta_t(\tau_p, n_*)$. Above θ_c there is no pair balance and at θ_t the plasma becomes effectively thick. Below the dotted curves pairs dominate ($z > 1$). The allowed parameter space depends weakly on n_* and can be divided into four characteristic regions: (I) optically thin ($\tau_T < 1$); (III) moderate Comptonization ($\tau_T > 1$ and $y_1 < 1$); (IV) and (V) saturated Comptonization ($y_1 > 1$). In region V double Compton dominates the photon production, while elsewhere bremsstrahlung dominates. The dashed curve shows the Thomson optical depth τ_T of the high-z solution for $\tau_p = 10^{-3}$ and $n_* = 10^{-10}$.

thick solid curves in Fig. 3 enclose the τ_p–θ parameter space of the high-z solutions for $n_* = 10^{-10}$. Below the dotted curve the plasma is pair-dominated ($z > 1$). In region I the Thomson optical depth τ_T is less than unity. Here optically thin bremsstrahlung dominates the radiation field. In region III moderate Comptonization of bremsstrahlung photons occurs ($\tau_T > 1$ but $y_1 < 1$), while in region IV saturated conditions are reached ($y_1 > 1$). At high enough radiation densities double Compton scattering provides the soft photons (region V). The weak dependence on n_* is seen from the dot-dashed curve in Fig. 2, representing the high-z branch for $\tau_p = 10^{-3}$ and $n_* = 10^{-10}$. The corresponding Thomson scattering optical depth, τ_T, (including pairs) is shown by the dashed curve in Fig. 3. The maximum possible τ_T in effectively thin pair-dominated plasmas is about 110 for $n_* = 10^{-10}$ and about 200 for $n_* = 10^{-20}$.

When photon–photon interactions dominate the pair production ($\tau_T \gtrsim 1$) and Comptonization occurs ($\tau_T \gtrsim 1$) at mildly relativistic temperatures an analytical analysis of the pair balance solutions is possible. For bremsstrahlung-dominated plasmas equation (3.7) can be explicitly solved for r leaving two algebraic equations to be solved for z and x_m. As the dependence on x_m is weak a first-order analysis requires the solving of only one equation for $z(\theta, \tau_p, x_m)$ (see Section 3.3). For double Compton-dominated plasmas

both r and x_m (here the dependence on x_m is of crucial importance) are solved for explicitly leaving only one equation to be solved for $z(\theta, \tau_p, n_*)$ (see Section 3.4).

3.2 WIEN EQUILIBRIUM PLASMAS (WEPs)

On a microscopic level Wien equilibrium demands (approximate) detailed balance for Compton scattering ($\gamma e \rightleftarrows \gamma e$) and photon–photon pair production/pair annihilation ($\gamma\gamma \rightleftarrows e^+e^-$) only. Pair-dominated WE cannot occur at relativistic temperatures as the photon–electron pair production rate (equation B10) would exceed the photon–photon rate (equation B6) for $\theta \gtrsim 4$. Furthermore the photon spectrum for $\theta^{-1} < x \lesssim \theta$ (the flat part above pair production threshold) does not have a Wien shape, and photon–photon interactions between the 'flat' photons and the Wien photons limit the possible existence of WEPs in our bremsstrahlung-dominated case to $\theta \lesssim 1$.

At each photon energy there is a detailed balance in WE,

$$\dot{n}_A(x, \theta)\, dx = c a_{\gamma\gamma}(x\theta)\, n(x, \theta)\, dx \tag{3.9}$$

and

$$\dot{n}_{cs}(x, \theta)\, dx = c a_{cs}(x, \theta)\, n(x, \theta)\, dx, \tag{3.10}$$

where $n(x, \theta)$ is the Wien distribution (equation 3.5), $a_{\gamma\gamma}(x\theta)\ \mathrm{cm}^{-1}$ is the photon–photon absorption coefficient (equations 14–18 in Svensson 1983), $a_{cs}(x, \theta)\ \mathrm{cm}^{-1}$ the Compton scattering opacity (equation 62 in S82), $\dot{n}_A(x, \theta)\ \mathrm{cm}^{-3}\ \mathrm{s}^{-1}$ the pair annihilation emissivity and $\dot{n}_{cs}(x, \theta)\ \mathrm{cm}^{-3}\ \mathrm{s}^{-1}$ the Compton scattering emissivity. For photon energies where $a_{\gamma\gamma}(x\theta) > a_{cs}(x, \theta)$ one also has $\dot{n}_A(x, \theta) > \dot{n}_{cs}(x, \theta)$ (see fig. 3 in Ramaty, McKinley & Jones 1982 for the case $\theta \approx \frac{1}{2}$). The detailed balance in equations (3.9) and (3.10) is not satisfied for photon energies where $\max[\tau_{\gamma\gamma} = a_{\gamma\gamma}R,\ \tau_{cs} = a_{cs}R] < 1$. Once the absolute values of n_+ and n_γ are known from the pair balance solutions a self-consistency check can be made. For the case $\tau_p = 10^{-3}$, $R = 10^{14}$ cm, and pair dominance ($z > 1$) we find that only for $\theta \lesssim 0.4$ (somewhat dependent on the chosen parameters τ_p and R [or n_*]) are the optical depths greater than unity at pair-producing photon energies. When few pairs are present ($z \ll 1$) at mildly relativistic temperatures the corresponding requirement is approximately $\tau_p \gtrsim 3$. The analytical treatment of a WEP below is thus limited by these constraints.

In a pair-dominated WEP the Wien distribution is established predominantly by photon–photon absorption/pair annihilations (equation 3.9) above a photon energy x_c (determined by $a_{\gamma\gamma}[x_c\theta] = a_{cs}[x_c, \theta]$) and by Compton scatterings (equation 3.10) below x_c. In fig. 3 of Ramaty *et al.* (1982) $x_c \approx 3$ for $\theta \approx \frac{1}{2}$ and it can be shown that x_c approaches unity as $[1 - \theta \ln(1.6/\theta)]^{-1}$ for $\theta \ll 1$. In a WEP with few pairs ($z \ll 1$) Compton scatterings dominate at pair-producing photon energies in establishing the Wien distribution.

Pair balance implies that the rate at which photons are absorbed in pair productions equals the rate at which annihilation photons are produced ($=2\dot{n}_A$). When Comptonization is negligible ($\tau_T \lesssim 1$ or, equivalently, $\theta \gtrsim 5$ for $z \gg 1$ [see Fig. 3]; $\tau_p \lesssim 1$ for $z \ll 1$) then the bremsstrahlung emissivity dominates the pair annihilation emissivity (either due to the 'Klein–Nishina' decline of the cross-section [$\theta \gtrsim 5$, $z \gg 1$] or due to lack of pairs [$\tau_p \lesssim 1$, $z \ll 1$]) and the absorption optical depth (due to pair production) is much less than unity making it unnecessary to include annihilation photons and photon absorption. In a pair-dominated WEP ($\theta \lesssim 0.4$, $z \gg 1$) on the other hand, the pair annihilation emissivity and photon–photon absorption are of crucial importance at photon energies larger than

x_c. The photon distribution above x_c follows directly from detailed balance (equation 3.9) eliminating the need for a detailed radiative transfer calculation. Furthermore, pair annihilations are not included as a source term in the photon balance equation (3.7) as the net production rate of photons from pair annihilations and photon–photon absorptions is zero.

For temperatures $0.4 \lesssim \theta \lesssim 5$ in a pair-dominated plasma and for $1 \lesssim \tau_p \lesssim 3$ in a plasma with few pairs the photon distribution at pair-producing energies is neither Wien nor optically thin bremsstrahlung. Here $\tau_T > 1$ allowing Compton scatterings to distort the bremsstrahlung spectrum but max $[\tau_{\gamma\gamma}, \tau_{cs}] < 1$ at pair-producing energies not allowing for the establishment of WE. For $z \gg 1$ the photon distribution around $x = \theta$ reflects the kinematics of the last Compton scattering of soft photons into this energy range as well as the cancelling effects of photon–photon absorption and annihilation emission. The peak of the photon distribution is therefore expected to shift to somewhat softer energies as compared with a Wien peak. Although our simplified treatment does not account for this change in spectral shape, the effect on the magnitude of the pair production rate (and on the pair density solutions) is not expected to be large.

We obtain the following qualitative picture of a pair-dominated WEP. A typical photon is produced at soft energies either by bremsstrahlung from the pairs or by double Compton scattering of the photons in the Wien peak against the pairs. Compton scatterings against the pairs rapidly brings the soft photon in to the Wien peak, where it stays while slowly diffusing out of the plasma. Occasionally, however, the photon may scatter into the Wien tail above x_c, where it will 'turn into' a particle (i.e. pair produce). As the photon re-emerges in the subsequent pair annihilation, it may, depending upon its energy x, either be more likely to scatter back into the Wien peak ($x < x_c$) or to pair produce again ($x > x_c$). The small number of pairs (relative to photons) present in the 'photon cloud' is just temporarily reconverted photons, which in the shape of pairs produce soft photons and Comptonize these into the Wien peak to replace those escaping from the cloud. The pairs, furthermore, provide the scattering medium for the photons, prolonging their escape.

3.3 BREMSSTRAHLUNG-DOMINATED WEPs

In a WEP the pair balance equation (3.1) reduces to

$$z + z^2 = r^2 \frac{\pi}{8\theta^3} \exp(-2/\theta)\, g_{WE}, \tag{3.11}$$

(using equations 2.8, 3.4, 3.8 and B5) relating the pair density z to the density r of Wien photons. For $\theta \lesssim 0.4$ only ep and e^+e^- bremsstrahlung are important, and using the non-relativistic spectral emissivities (Appendix A) the solution of the photon balance equation (3.7) becomes

$$r = (1 + 2z)[(1 + 2z) + 2^{3/2}(z + z^2)]\tau \frac{2}{\rho}\alpha\left(\frac{2}{\pi}\right)^{3/2}\theta^{-1/2}\frac{1}{2}\ln^2(\theta/x_{coh})\,\xi f_B g_\tau, \tag{3.12}$$

where x_{coh} is the solution to equation (D1d). Eliminating r in the pair balance equation then gives

$$z + z^2 = (1 + 2z)^2\,[(1 + 2z) + 2^{3/2}(z + z^2)]^2\, G(\theta, \tau_p, n_*, z), \tag{3.13}$$

where

$$G(\theta, \tau_p, n_*, z) = \left(\frac{\alpha}{2\pi}\right)^2\left(\frac{\tau_p}{\theta}\right)^4 \ln^4\left(\frac{\theta}{x_{coh}}\right)\exp(-2/\theta)(\xi f_B g_\tau)^2\, g_{WE}. \tag{3.14}$$

The dependence of G on n_* and z (through $x_{\rm coh}$ and $f_{\rm B}$) is weak. Neglecting this dependence on z it is found that for $G > G_{\rm c} \equiv 3.35 \times 10^{-2}$ there exist no real solutions of equation (3.13), while at $G < G_{\rm c}$ there are two positive real solutions. Then from equation (3.14) it follows that for each set of θ and n_* there exists a maximum value of $\tau_{\rm p}$ beyond which there are no solutions,

$$\tau_{\rm p}^{\rm max} = G_{\rm c}^{1/4}\left(\frac{2\pi}{\alpha}\right)^{1/2} \theta \exp(1/2\theta)[\ln(\theta/x_{\rm coh})]^{-1}(\xi f_{\rm B} g_\tau)^{-1/2} g_{\rm WE}^{-1/4}, \tag{3.15}$$

which is a decreasing function of θ for temperatures considered here ($\theta \lesssim 0.4$). $\tau_{\rm p}^{\rm max}(\theta, n_* = 10^{-10})$ is shown in Fig. 3 as the upper thick boundary of region IV. Inversely, for each set of $\tau_{\rm p}$ and n_* there exists a maximum temperature $\theta_{\rm c}(\tau_{\rm p}, n_*)$ beyond which there is no steady pair density. At $\theta < \theta_{\rm c}$ the pair balance equation has a low-z solution, $z = G \propto \theta^{-4} \exp(-2\theta)(\xi f_{\rm B})^2$, and a high-$z$ solution, $z = 2^{-5/4} G^{-1/4} \propto \theta \exp(1/2\theta)(\xi f_{\rm B})^{-1/2}$. The branches merge at $\theta = \theta_{\rm c}$ where $z \approx 0.106$ (again neglecting the weak z-dependence of G) as long as $\theta_{\rm c} \lesssim 0.4$ (or $\tau_{\rm p} \gtrsim 2$–3). For smaller $\tau_{\rm p}$ the high-z branch only is in WE for $\theta \lesssim 0.4$. Along these high-z branches the Thomson scattering optical depth $\tau_{\rm T}$ is

$$\tau_{\rm T} = 2z\tau_{\rm p} = 2^{1/4}(\pi/\alpha)^{1/2}\theta \exp(1/2\theta)[\ln(\theta/x_{\rm coh})]^{-1}(\xi f_{\rm B} g_\tau)^{-1/2} g_{\rm WE}^{-1/4} \qquad (z \gg 1, \quad \tau_{\rm p} \ll 1), \tag{3.16}$$

which decreases monotonically with temperature over its range of validity ($\theta \lesssim 0.4$). The dashed curve in Fig. 3 shows $\tau_{\rm T}$ for $\tau_{\rm p} = 10^{-3}$ and $n_* = 10^{-10}$. The high-z branches become effectively thick when r and z reach their TE-values (equations 2.4 and 2.1) at $\theta_{\rm t}(\tau_{\rm p}, n_*)$ or, inversely, $\tau_{\rm p}^{\rm min}(\theta, n_*)$. For $z \gg 1$ equation (3.12) gives

$$\tau_{\rm p}^{\rm min} = n_*[\zeta(3)/\alpha]^{1/2}\pi^2 2^{-1/4}\theta^{-1/2} \exp(3/2\theta)[\ln(\theta/x_{\rm coh})]^{-1}(\xi f_{\rm B} g_\tau g_{\rm TE}^{3/2})^{-1/2} \qquad (z \gg 1). \tag{3.17}$$

Fig. 3 shows $\tau_{\rm p}^{\rm min}(\theta, n_* = 10^{-10})$ as the lower thick boundary of region IV.

Changing geometry from spherical to slab (half thickness h and $\tau_{\rm p} = n_{\rm p}\sigma_{\rm T} h$) causes ξ to increase by about a factor of 3. The geometry sensitive low-z branch increases by a factor of $\xi^2 \approx 10$, while most other aspects of the pair balance solutions change by less than a factor of 2. When saturation is moderate there is also a ξ-dependence through $f_{\rm B}$.

The simplified treatment in this section showed the main features of the pair balance solutions when WE is maintained and bremsstrahlung dominates. For $\theta \lesssim 0.1$, however, the photon densities become large enough for double Compton scatterings to become important.

3.4 DOUBLE COMPTON-DOMINATED WEPs

The photon production rate, $\dot{n}_\gamma^{\rm DC}$, from double Compton scatterings dominates over the corresponding rate for bremsstrahlung, $\dot{n}_\gamma^{\rm B}$, in providing Wien photons when $f_{\rm DC}\dot{n}_\gamma^{\rm DC} > f_{\rm B}\dot{n}_\gamma^{\rm B}$. Double Compton is only important for saturated Comptonization and $f_{\rm DC} \approx f_{\rm B} \approx 1$. For $z \ll 1$ e^-p interactions are the main bremsstrahlung mechanism and using the rates in Appendix A gives (*cf.* equation 19 in L81, which differs by a factor 4π)

$$\frac{\dot{n}_\gamma^{\rm DC}}{\dot{n}_\gamma^{\rm B}} = r\left(\frac{\pi}{2}\right)^{1/2} 16\theta^{5/2}[\ln(4\eta\theta/x_{\rm coh})]^{-1} g_{\rm DC} > 1 \qquad (z \ll 1, \quad \theta \lesssim 1), \tag{3.18}$$

for double Compton to be dominant (g_{DC} is a relativistic correction factor given by equation A10a). In WE there is a definite relationship between r and z and equation (3.18) can be written as a condition on z using the low-z limit of equation (3.11),

$$z > 2^{-10}\theta^{-8}\exp(-2/\theta)\ln^2(4\eta\theta/x_{coh})\,g_{WE}g_{DC}^{-2} \qquad (z \ll 1, \qquad \theta \leqslant 1). \tag{3.19}$$

In a pair-dominated plasma double Compton competes with e^+e^- bremsstrahlung giving

$$\frac{\dot{n}_\gamma^{DC}}{\dot{n}_\gamma^{B}} = \frac{r}{z}\,8\pi^{1/2}\theta^{5/2}\left[\ln(4\eta\theta/x_{coh})\right]^{-1} g_{DC} > 1 \qquad (z \gg 1, \qquad \theta \leqslant 1), \tag{3.20}$$

for double Compton to dominate. As r/z in a pair-dominated WEP is a function of temperature only (equation 3.11) equation (3.20) becomes a condition on θ only (with a very weak dependence on x_{coh}),

$$\theta < 1/\ln\left[(2^{1/2}16\theta^4)^{-1}\ln(4\eta\theta/x_{coh})\,g_{WE}^{1/2}\,g_{DC}^{-1}\right] \tag{3.21}$$

or $\theta < 0.11$ for any reasonable value of x_{coh}. The transition to double Compton dominance is easily noticeable in Fig. 2, where the high-z branches show a bend at $\theta \simeq 0.1$.

L81 discussed in detail the double Compton process in finite, strongly Comptonized, non-relativistic plasmas without pairs. His results are easily generalized to include pairs and relativistic corrections. The photon balance equation (3.7) becomes

$$n_\gamma = n_\gamma\alpha\,\frac{16}{\pi}\,\tau_T^2\,\theta^2\ln(\theta/x_{coh})\,\xi g_\tau g_{DC} \qquad (\theta \leqslant 1), \tag{3.22}$$

where x_{coh} is obtained by solving equation (D1d)

$$x_{coh} = (2\pi\alpha n_\gamma \lambda\!\!\!^{-3} g_{DC})^{1/2} \qquad (\theta \lesssim 1/8) \tag{3.23}$$

(*cf.* equation 25 in L81). The crucial feature of double Compton-dominated plasmas is that both the photon escape rate and the photon production rate are proportional to n_γ as is seen in equation (3.22). The only remaining n_γ dependence is in x_{coh} in the logarithmic factor. For small changes in τ_T or θ steadiness can only be maintained if n_γ changes exponentially,

$$n_\gamma = \lambda\!\!\!^{-3}(\theta^2/2\pi\alpha)\exp\left[-\pi/(8\alpha\tau_T^2\theta^2\xi g_\tau g_{DC})\right] g_{DC}^{-1} \qquad (\theta \lesssim 1/8) \tag{3.24}$$

(*cf.* equation 72 in L81). From equations (3.11) and (3.24) pair balance gives

$$z + z^2 = n_*^{-2}(32\pi\alpha^2)^{-1}\,\theta\exp\left[-(2/\theta) - \pi/(4\alpha\tau_T^2\theta^2\xi g_\tau g_{DC})\right] g_{WE}g_{DC}^{-2} \qquad (\theta \lesssim 1/8), \tag{3.25}$$

or, equivalently,

$$\begin{aligned}\tau_T &= \tau_p(1+2z)\\ &= (\pi/4\alpha)^{1/2}\left[\!\left[-\theta^2\ln\left[n_*^2 32\pi\alpha^2(z+z^2)\,\theta^{-1}g_{WE}^{-1}g_{DC}\right] - 2\theta\right]\!\right]^{-1/2}(\xi g_\tau g_{DC}^2)^{-1/2},\end{aligned} \tag{3.26}$$

which is to be solved for z as a function of θ, τ_p and n_*. The low-z solution is directly obtained from equation (3.25) by neglecting the z^2-term on the left-hand side and by replacing τ_T with τ_p on the right-hand side. The very strong dependence on θ at small z is shown by the $\tau_p = 10^2$ curve in Fig. 2. The high-z solution cannot be obtained in explicit form, but equation (3.26) can be rewritten as an implicit equation for $\tau_T(\theta, R)$ independent of the proton density n_* as expected for a pair-dominated plasma.

Similar to the bremsstrahlung case there is a maximum τ_p (for given θ and n_*) beyond which there is no steady pair balance. Regarding τ_p as a function of z, then differentiating equation (3.26) to find τ_p^{max} gives

$$(\tau_p^{max})^2 = \frac{\pi}{\alpha}\theta^{-2}(z_c + z_c^2)(1 + 2z_c)^{-4}(\xi g_\tau g_{DC})^{-1}, \tag{3.27}$$

where $\tau_p^{max} = \tau_p(z_c)$. Using the fact (see Fig. 2) that $z_c \approx 10^{-2} \ll 1$ and eliminating z_c from equations (3.26) and (3.27) gives

$$\tau_p^{max} = (\pi/4\alpha)^{1/2}[\![-\theta^2 \ln [n_*^2 32\alpha^3\theta(\tau_p^{max})^2 \xi g_{WE}^{-1} g_\tau g_{DC}^3] - 2\theta]\!]^{-1/2}(\xi g_\tau g_{DC})^{-1/2}. \tag{3.28}$$

The solution $\tau_p^{max}(\theta, n_* = 10^{-10})$ or, inversely, $\theta_c(\tau_p, n_* = 10^{-10})$ is shown in Fig. 3 by the upper thick boundary of region V.

The high-z branches become effectively thick when r and z reach their TE-values (equations 2.4 and 2.1) at $\theta_t(\tau_p, n_*)$ or, inversely, $\tau_p^{min}(\theta, n_*)$. For $z \gg 1$, equation (3.22) gives

$$\tau_p^{min} = n_* \tfrac{1}{4}\pi^2 \alpha^{-1/2}\theta^{-5/2} \exp(1/\theta)\{\ln [\![\pi/[4\alpha\zeta(3)\theta g_{DC}]]\!] \xi g_\tau g_{DC} g_{TE}\}^{-1/2} \qquad (z \gg 1), \tag{3.29}$$

shown in Fig. 3 as the lower thick boundary of region V. The τ_p^{min} and τ_p^{max} boundaries in Fig. 3 join at $\theta_{min}(n_*)$ determined (using equations 2.1, 3.25, and 3.27) by

$$\theta_{min} = 2/\ln [\![2\pi^{-3} n_*^{-2}\theta_{min}^3 \ln [\pi^2(4\alpha\theta_{min})^{-2} g_{WE} g_{DC}^{-2} g_{TE}^{-1}] g_{TE}]\!]. \tag{3.30}$$

The one possible steady pair density at $\theta < \theta_{min}$ is necessarily less than $z_c \approx 10^{-2}$, and pairs are always unimportant in steady plasmas for $\theta < \theta_{min}$.

In effectively thick conditions where double Compton dominates ($\theta \lesssim 0.1$) one has $x_{coh}/\theta \approx 0.14\theta^{1/2} \ll 1$. Thus the Planckian radiation field is never completely self-absorbed due to the double Compton process, but it is maintained at $x > x_{coh}$ by direct and inverse Compton scatterings (see Thorne 1981 for a detailed discussion).

3.5 COMPARISON WITH OTHER WORK

Stoeger (1977) considered pair balance in fully saturated ($f_B = 1$) bremsstrahlung-dominated WEPs in the temperature range $0.1 < \theta < 1$ and for $\tau_p \approx 1.3$ and 13. As the low-z solution was used even when $z > 1$ the existence of a maximum temperature $\theta_c(\tau_p)$ was not found. In fact for $\tau_p \approx 13$ no solutions exist in the temperature range Stoeger studied as $\theta_c \approx 1$.

Yahel (1982) determined the pair density in a three-layer cloud by iterating between solving the radiative transfer problem using Monte Carlo methods and solving the pair balance equation for each layer. The results (pair density, emerging spectrum, luminosity) from the second iteration were presented for nine different choices of parameters. In the dominant intermediate layer having an outer radius $R = 5 \times 10^{13}$ cm the chosen parameters were $\theta \approx 0.8$ or 2 and $\tau_p \approx 1$ or 10. There is a strong disagreement between Yahel's and our results. For $\tau_p = 10$ we find that there do not exist any effectively thin steady solutions at either $\theta \approx 0.8$ or 2 as $\theta_c \approx 0.1$ (see Fig. 2), while Yahel obtains $z \approx 200$–500. Continued iterations would have caused z to continue to increase until effectively thick conditions are reached at z of order 10^{20}. In at least five of the nine models we conclude that the presented results do not represent the solutions to the posed steady state problem.

Stepney (1983) used a time-dependent radiative transfer code to let the pair density of a slab at a fixed temperature evolve to its steady value (if $\theta < \theta_c$), thereby obtaining the

low-z solution branch (the high-branch being unstable to isothermal perturbations). The solution curves for $0.01 < z < 0.1$ differ in temperature by about a factor of 2 or less from our results for $1/3 < \tau_p < 1$. There is also agreement as regards the values of z (≈ 0.1) at θ_c. However, the slopes of $\tau_p^{max}(\theta)$ in Stepney's temperature range $0.6 < \theta < 1.6$ differ indicating that the discrepancies between the results of the two methods would increase at larger and smaller temperatures.

Zdziarski (1984a, b) used the Monte Carlo method to determine the radiation field in a spherical cloud of given θ, τ_p, n_* and z. The net pair production rate was calculated and the value of z giving zero net pair production (i.e. pair balance) was obtained iteratively, allowing for the determination of *both* the high- and low-z branches. The obtained solutions for $\theta > 0.15$ and $10^{-3} < \tau_p < 10^{0.5}$ differ in temperature by less than a factor of 2 from our results.

These two latter works complement that of this paper in that for a restricted set of parameters θ, τ_p and n_* a very detailed study of the properties throughout the cloud can be made, especially as regards spectral shape, absorption, anisotropy and non-homogeneity.

4 Classification of steady mildly relativistic plasmas

Combining the results in previous sections with those on Comptonization of bremsstrahlung (Felten & Rees 1972; Illarionov & Sunyaev 1972) and of double Compton radiation (L81) in non-relativistic plasmas, it is possible to divide the $\tau_p - \theta$ parameter space at fixed n_* into the 11 regions listed in Table 1 and shown in Figs 3 and 4. The conditions and the straightforwardly derived expressions determining the location of the boundaries of the regions are given in Table 2 together with some notational comments.

Pair production effects cause the region of parameter space outlined by the thick boundaries in Fig. 3 to have two effectively thin states (the low-z and the high-z solutions of Section 3) and one effectively thick state (TE). Fig. 3 classifies the high-z solutions, while Fig. 4 classifies the low-z solutions in this 'multi-valued' part of parameter space. A plasma is effectively thin below and effectively thick above the thick dashed and the thick solid curve in Fig. 4, while the high-z states of Fig. 3 are all effectively thin. Another major division occurs along the dotted curves where $n_+ = n_p$. Pairs dominate (by number) below the dotted curve in Fig. 3 and to the right of the dotted line (θ_+) in Fig. 4. The position of the θ_+ line is determined using equation (2.1) in the non-relativistic limit,

$$\theta_+ = 2/\ln[2n_*^{-2}(\theta_+/2\pi)^3]. \tag{4.1}$$

Table 1. Regions in $\tau_p - \theta$ parameter space.

Region	Local spectrum	Dominant processes
I	Bremsstrahlung	Bremsstrahlung
II	Bremsstrahlung	Bremsstrahlung, coherent scattering
III	Wien	Bremsstrahlung, moderate Comptonization
IV	Wien	Bremsstrahlung, saturated Comptonization
V	Wien	Double Compton, saturated Comptonization
VI	Planck	Bremsstrahlung, free–free absorption
VII	Planck	Bremsstrahlung, free–free absorption, coherent scattering
VIII	Planck	Bremsstrahlung, Comptonization
IX	Planck	Double Compton, Comptonization
X	Planck	Bremsstrahlung, Comptonization
XI	Planck	Bremsstrahlung, free–free absorption

Table 2. The boundaries in $\tau_p-\theta$ parameter space. The photon energies x_{abs}, x_t, x_0, and x_{coh} are discussed in Appendix D. For $z \ll 1$ and $\theta \ll 1 x_{coh} = 0.068 n_* \theta^{-5/4} \ln (2.25\theta/x_{coh})$, while for $z \gg 1$ the right-hand side should be multiplied by $1.2 z^{1/2}$. The photon density n_γ^{TE} and the pair density n_+^{TE} (for $n_+ \gg n_p$) in TE are given by equations (2.4) and (2.1), respectively. The steady photon densities n_γ^B and n_γ^{DC} are the solutions of equation (3.7) in the non-relativistic limit when bremsstrahlung and double Compton, respectively, dominate. The normal (y) and the 'saturated' (y_1, f_B) Comptonization parameters are defined in Appendix C. The geometry factor ξ is discussed in Section 2.2 and Appendix C. The relativistic correction factors g_τ (equation B13), g_{DC} (equation A10a), and g_{WE} (equation 2.9) are included where necessary. Planckian photons below x_{coh} were included in the determination of boundary IV–VIII. The soft emissivities were used in the $x = \theta$ conditions (except for the X–XI boundary), and using the exact emissivities will give slightly different numerical factors.

Boundary	Conditions	Expression
I–II, I–III	$\tau_T = 1$	$\begin{cases} \tau_p = 1 & (z \ll 1) \\ \theta \approx 6 & (z \gg 1) \end{cases}$
I–IV	$x_{abs} = \theta$	$\tau_p = 34 n_*^{-1} \theta^{7/2}$
II–III	$y = 1/2$	$\tau_p = 0.35\, \theta^{-1/2}$
II–VII	$x_t = \theta$	$\tau_p = 5.8 n_*^{-1/2} \theta^{7/4}$
III–IV	$y_1 = 1$	$\tau_p = \ln^{1/2}(\theta/x_{coh})[\xi \ln(1 + 4\theta + 16\theta^2)]^{-1/2}$ $(z \ll 1)$
IV–V	$\dot{n}_\gamma^B = \dot{n}_\gamma^{DC}$	$\begin{cases} \tau_p = 7.3\theta^{-1}[2 \ln(2.25\theta/x_{coh})\, \xi g_\tau g_{DC}]^{-1/2} & (z \ll 1) \\ \theta = [\![\ln[0.044\theta^{-4} \ln(2.25\theta/x_{coh})\, g_{WE}^{1/2} g_{DC}^{-1}]]\!]^{-1} \approx 0.11 & (z \gg 1) \end{cases}$
IV–VIII	$n_\gamma^B = n_\gamma^{TE}$	$\begin{cases} \tau_p = 11 n_*^{-1/2} \theta^{7/4} [\ln(2.25\theta/x_{coh})]^{-1} \\ \quad \times [1 - (x_{coh}/\theta)^2]^{1/2} (\xi f_B)^{-1/2} \end{cases}$
V–IX	$n_\gamma^{DC} = n_\gamma^{TE}$	$\tau_p = 7.3\theta^{-1}[\![\ln[90/(\theta g_{DC})]\, \xi g_\tau g_{DC}]\!]^{-1/2}$
VI–VII	$x_0 = \theta$	$\theta_L^{cs} = 0.37 n_*^{2/7}$
VII–VIII	$x_{coh} = \theta$	$\theta_L^B = 0.29 n_*^{2/9}$
VIII–IX	$\dot{n}_\gamma^B = \dot{n}_\gamma^{DC}$, $n_\gamma = n_\gamma^{TE}$	$\theta_L^{DC} = 0.66[\![n_* \ln[90/(\theta_L^{DC} g_{DC})]\, g_{DC}^{-1}]\!]^{2/11}$
IX–X	$\dot{n}_\gamma^B = \dot{n}_\gamma^{DC}$, $n_\gamma = n_\gamma^{TE}$, $n_+ = n_+^{TE}$	$\theta_U^{DC} = 0.12$
X–XI	$x_{coh} = \theta$, $n_+ = n_+^{TE}$	$\theta_U^{cs} = \theta_U^B = 2.5$

The plasma is effectively thick at all temperatures for τ_p larger than its value at point c in Fig. 4,

$$(\tau_p)_c = 11 n_*^{-2/11}\{\ln[\![71[(\tau_p)_c^2 \xi/n_*]^{2/15}]\!]\}^{-15/22} \xi^{-1/2}, \tag{4.2}$$

valid when the double Compton-dominated region V exists ($n_* < 10^{-6}$, see below), and having values roughly from 10^2 to 10^5 for n_* ranging from 10^{-6} to 10^{-24}. For plasmas with $\tau_p > (\tau_p)_d$ the steady pair density z is a monotonically increasing function of temperature θ. For given $\tau_p < (\tau_p)_d$ the plasma moves to larger temperature as z increases until the thick solid curve, $\theta_c(\tau_p, n_*)$, is reached. Increasing z further moves the plasma into the parameter space of Fig. 3, where the temperature decreases with z until effectively

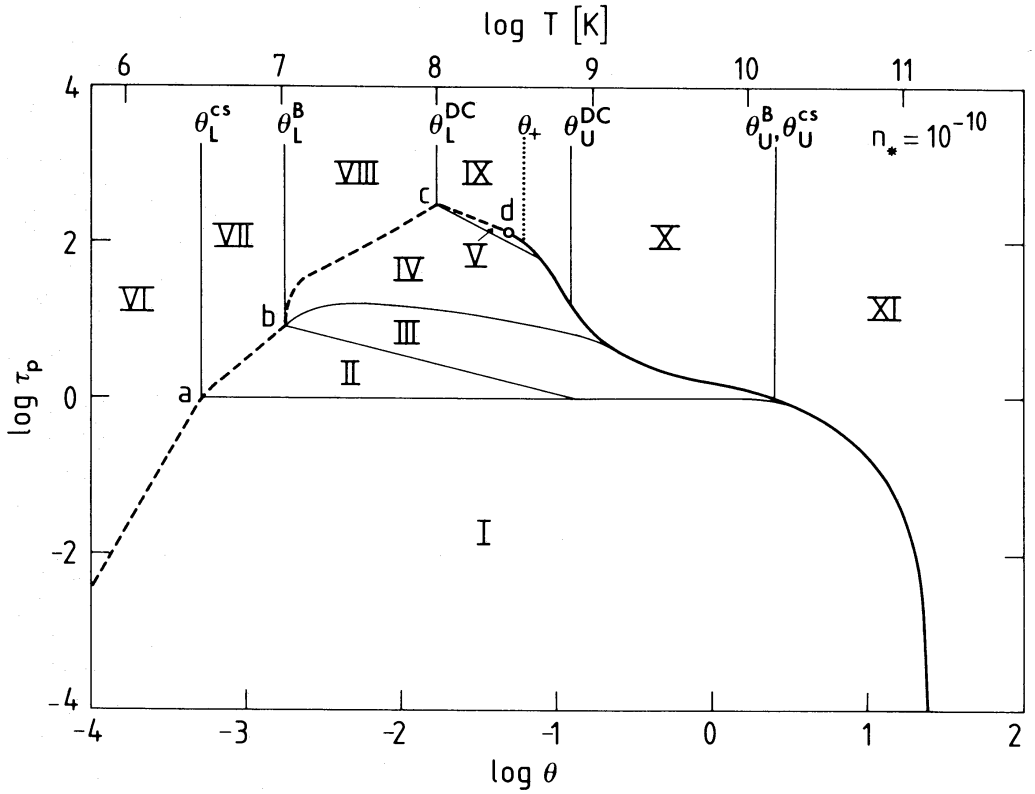

Figure 4. The τ_p–θ parameter space of a steady plasma for $n_* = 10^{-10}$. The regions, their dominant processes, and their boundaries are given in Tables 1 and 2. Pairs dominate ($z > 1$) to the right of the dotted curve. The plasma is effectively thick above and effectively thin below the thick dashed and solid curve. The plasma cannot cross the thick solid curve but instead moves into the effectively thin high-z parameter space in Fig. 3 if the thick curve is approached from regions I–V. The narrowness of region V is caused by the extreme sensitivity of the steady photon density in double Compton-dominated plasmas to changes in τ_p and θ.

thick conditions (at $\theta_t[\tau_p, n_*]$) are approached. The plasma once again moves to larger temperature as z increases and eventually back into Fig. 4 to the right of the thick solid curve.

The boundary curves I–II, II–III, and IV–V are independent of n_* and the points a, b($[\tau_p]_b = 0.66 n_*^{-1/9}$), and c move along these curves when n_* changes (to the right for increasing n_*). Therefore the effectively thin regions (I–V) diminish as n_* increases. The behaviour of the effectively thick boundaries θ_L^{cs}, θ_L^B, θ_L^{DC}, θ_U^{DC}, θ_U^B, and θ_U^{cs} between regions VI and XI with changing n_* is shown in Fig. 5 (*cf.* fig. 1 in Thorne 1981 for non-relativistic temperatures) and the corresponding expressions are given in Table 2. The plasma is pair dominated above $\theta_+(n_*)$ and degenerate below

$$\theta_{deg} = [1 + (3\pi^2 n_*)^{2/3}]^{1/2} - 1. \tag{4.3}$$

In most of the θ–n_* parameter space (regions VIII, IX, X) Comptonization of soft photons establishes the Planckian radiation field. L81 and Thorne (1981) showed that above θ_L^{DC} double Compton scattering dominates bremsstrahlung in producing soft photons. Here we find that once the plasma is pair dominated enough, pairs will re-establish the dominance of bremsstrahlung (at $\theta_U^{DC} \approx 0.12$). Furthermore, double Compton is never important for $n_* \gtrsim 10^{-6}$. Finally, the decline of the Compton cross-section at relativistic temperatures and the increase of pairs ($n_+ \propto \theta^3$) cause free–free emission and absorption ($\propto n_+^2$) to dominate over Comptonization ($\propto n_+$) above $\theta_U^B \approx 2.5$.

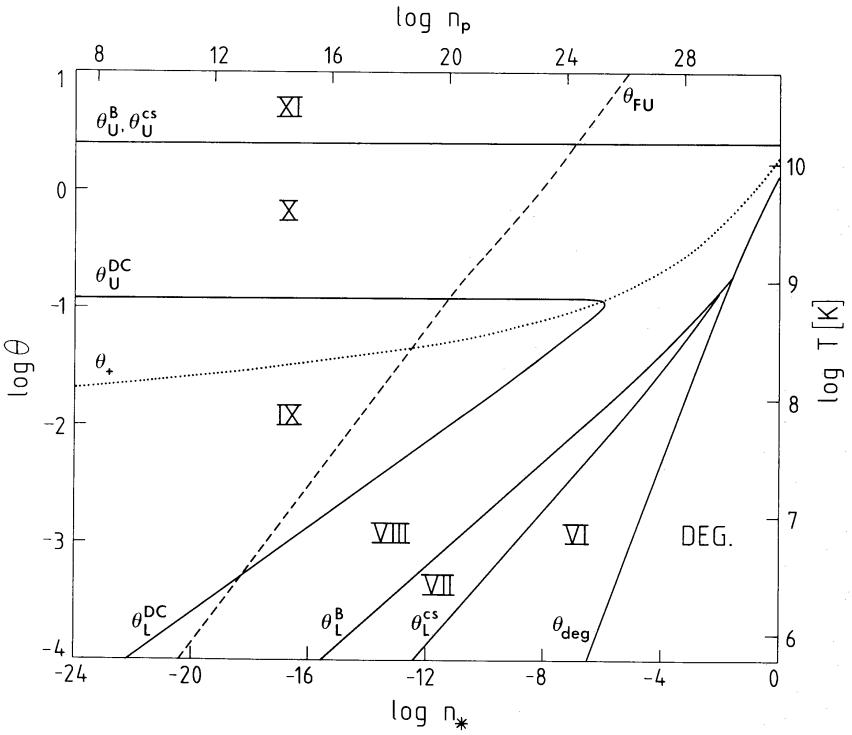

Figure 5. The $\theta - n_*$ parameter space of a plasma in thermodynamic equilibrium. The regions, their dominant processes, and their boundaries are given in Tables 1 and 2. Above θ_+ (the dotted curve) pairs dominate ($z > 1$), while below $\theta_{\rm deg}$ the plasma is degenerate. The path taken by a flat Friedmann universe is shown by $\theta_{\rm FU}$ (the dashed curve).

5 The luminosity from steady mildly relativistic plasmas

The dimensionless luminosity $l(\theta, \tau_{\rm p}, R)$ is shown in Fig. 6(a) ($R = 10^6$ cm) and Fig. 6(b) ($R = 10^{14}$ cm) as a function of θ for $10^{-4} < \tau_{\rm p} < 10^4$. While Table 3 gives simple expressions for l in various regimes. The luminosity (or cooling) curves for different $\tau_{\rm p}$ become independent of the proton optical depth $\tau_{\rm p}$ and join a unique single cooling curve when the plasma becomes pair dominated. For $l \lesssim 1$ optically thin bremsstrahlung cooling dominates, being $\propto \theta^{1/2}$ for $\theta \lesssim 1$ and $\propto \theta \ln \theta$ for $\theta \gtrsim 1$ as long as pairs are negligible. The optically thin luminosity curves do not depend on R as for two-body processes

Table 3. The luminosity from steady plasmas. $a_{\rm ff}$ is the mean free–free opacity, $a_{\rm T}$ is the Thomson scattering opacity, and $a_{\rm w}$ is given by equation (B12). See the text of Table 2 for some further notational comments.

Regions	Dimensionless luminosity	
I, II	$l = \begin{cases} \tau_{\rm p}^2 \alpha (16/3)(2\theta/\pi)^{1/2}(1 + 2.67\theta + 5.47\theta^2 - 2.46\theta^3) & (\theta \ll 1, z \ll 1) \\ \tau_{\rm p}^2 \alpha 18\theta[\ln(2\eta\theta + 0.14) + 4/3] & (\theta \gg 1, z \ll 1) \end{cases}$	
III, IV	$l = \tau_{\rm p}^2 \alpha 4(2\theta/\pi)^{1/2} \ln^2(4\eta\theta/x_{\rm coh})\, f_{\rm B}$	$(\theta \ll 1, z \ll 1)$
V	$l = R\sigma_{\rm T}\bar{\chi}^{-3}(2/\alpha)\,\theta^3 \tau_{\rm p}^{-1} \exp[-\pi/(8\alpha\tau_{\rm p}^2\theta^2 \xi g_\tau g_{\rm DC})](\xi g_\tau g_{\rm DC})^{-1}$	$(z \ll 1)$
IV, V	$l = l_{\rm WE} \equiv 4(2\pi)^{1/2}\theta^{5/2} \exp(1/\theta)(\xi g_\tau g_{\rm WE}^{1/2})^{-1}$	$(z \gg 1)$
VI, XI	$l = l_{\rm BB} \equiv R\sigma_{\rm T}\bar{\chi}^{-3}(\pi^3/15)\,\theta^4$	
VII	$l \approx l_{\rm BB}(a_{\rm ff}/a_{\rm T})^{1/2}$	
VIII, X	$l \approx l_{\rm BB}[\dot{n}_\gamma^{\rm B}/(ca_{\rm w} n_\gamma^{\rm TE})]^{1/2}$	
IX	$l \approx l_{\rm BB}[\dot{n}_\gamma^{\rm DC}/(ca_{\rm w} n_\gamma^{\rm TE})]^{1/2}$	

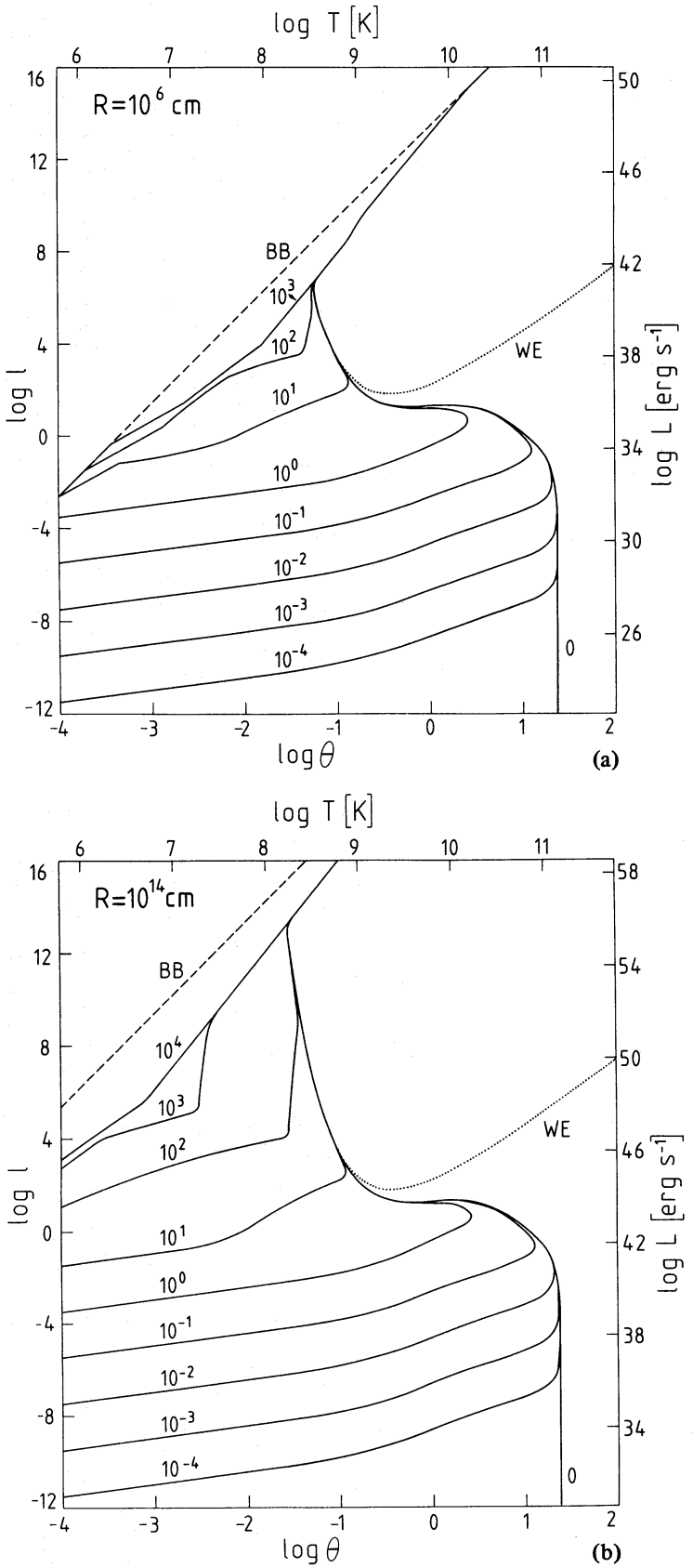

Figure 6. (a) The luminosity $L = lRmc^3/\sigma_T = lR\ 3.7 \times 10^{28}$ erg s^{-1} from a steady spherical plasma cloud of size $R = 10^6$ cm. The 'proton' optical depth, τ_p, labels each solid curve. The dashed line shows the luminosity from a black body and the dotted curve the luminosity from a pair-dominated plasma in Wien equilibrium. Pair-dominated Wien equilibria are realized only for $\theta \lesssim 0.4$. Along the $\tau_p = 10^3$ curve the plasma cloud is effectively thick, but due to scatterings the luminosity is suppressed relative to the black body luminosity. (b) Same as (a) but for $R = 10^{14}$ cm.

$L \propto R^3 n^2 \propto R\tau_T^2$ (neglecting temperature-dependent factors) and $l \propto L/R$ is independent of R. In a pair-free plasma $\tau_T = \tau_p$, and therefore $l = l(\theta, \tau_p)$, while in a pair-dominated plasma $\tau_T = \tau_T(\theta)$ and hence $l = l(\theta)$. For $l \gtrsim 1$ moderate and saturated Comptonization of soft bremsstrahlung and double Compton photons provides the cooling. The abrupt change in the behaviour of the cooling curves for $\tau_p = 10^2$ and 10^3 is caused by the onset of double Compton dominance. The exponential dependence of the Comptonized double Compton luminosity on temperature brings the plasma into effectively thick conditions after only a slight increase in temperature. It is clear from Fig. 6(a, b) that there exists a maximum $\tau_p(R)$ (or, equivalently, a maximum $\tau_p[n_*]$ given by equation 4.2) for which a plasma is effectively thin. Furthermore, over a range of temperatures ($\theta_L^{cs} < \theta < \theta_U^{cs}$) the effectively thick luminosity is reduced below the blackbody luminosity due to scattering effects as is shown in Fig. 6(a) and the last three entries in Table 3.

Pair production effects cause a large region in $l-\theta$ space to be forbidden for steady, stationary, thermal plasmas. This region is bounded by the pair-dominated cooling curve, whose behaviour at scattering optical depths $\tau_T \ll 1$ and $\tau_T \gg 1$ is obtained using very simple arguments. As shown by Bisnovatyi-Kogan, Zel'dovich & Sunyaev (1971) the requirement of pair balance, when particle–particle pair production dominates ($\tau_T \ll 1$), limit allowed temperatures to be less than θ_{max} determined by

$$\theta_{max} \ln \theta_{max} \approx \frac{\pi}{4\sqrt{2}\alpha} \tag{5.1}$$

or $\theta_{max} \approx 24$. At $\theta > \theta_{max}$ pair annihilations can never balance particle–particle pair productions independent of the amount of pairs present. When $\tau_T \gg 1$ the plasma is in WE and for a pair-dominated WEP the luminosity is given by $l_{WE}(\theta)$ (equation 2.13 and shown by the dotted curve in Fig. 6a, b) applicable for $\theta \lesssim 0.4$. The pair-dominated cooling curve for $0.4 \lesssim \theta < \theta_{max}$ can only be determined by using the pair balance results of Section 3. The resulting cooling curve is approximately constant, $l \approx 20$, for $1/3 \lesssim \theta \lesssim 3$. *Thus a luminosity larger than $L \approx 7 \times 10^{43} R_{14}$ erg s^{-1} can only emerge from a steady, thermal plasma cloud at subrelativistic ($\theta \lesssim 1/3$) temperatures.* (If one incorrectly assumes the validity of pair-dominated WE (the dotted curve) at all temperatures, then two temperature states, one low temperature ($\theta < 0.37$) and one high temperature ($\theta > 0.37$), are allowed at a given $l > 60$ (*cf.* the two pair-dominated branches in Fig. 1 in Liang 1979).)

The dimensionless Eddington luminosity of a pair-free plasma is $l_E = 2\pi(m_p/m)(R_s/R) \approx 1.2 \times 10^4 (R_s/R)$, where m_p is the proton mass and R_s is the Schwarzschild radius of the black hole trying to confine the cloud. The double Compton process is never of importance for $l \lesssim 2 \times 10^3$ and is therefore never dominant in Eddington limited plasmas with $R/R_s \gtrsim 5$. In pair-dominated plasmas the Eddington luminosity becomes $l_E^{pair} \approx 2\pi (R_s/R) g_{KN}(\theta) \lesssim 1.3 g_{KN}(\theta)$ for $R \gtrsim 5R_s$. The factor g_{KN}(=1 for $\theta \ll 1$) allows for Klein–Nishina corrections, depends on the spectral shape, and generally increases for $\theta > 1$. It follows from Fig. 6(a, b) that pair-dominated plasmas certainly exceed the Eddington limit for $\theta \lesssim$ a few. For $\theta \gtrsim$ a few the pairs are in any case relativistic and cannot be gravitationally confined. We conclude that *pair-dominated thermal plasmas are necessarily dynamical* (pair winds) *at all temperatures unless confined by a dynamically dominant magnetic field.* Then, however, efficient cyclosynchrotron radiation provides additional soft photons that once upscattered to $x \gtrsim 1$ produce pairs, which changes the details of the pair balance solutions (the pair density on the high-z branch decreases, while that on the low-z branch increases). Magnetic field strengths, B, much below equipartition values are sufficient to decrease $\theta_c(\tau_p, n_*, B)$, now a function of B also (Araki & Lightman 1983; Kusunose & Takahara 1983). For saturated Comptonization of cyclo-synchrotron photons

the luminosity of the plasma is simply $l_{WE}(\theta)$, as the luminosity in WE conditions is independent of the process producing the soft photons (for a strong enough soft photon source the photon spectrum at energies below 3θ may even have the power law shape of unsaturated Comptonization). The size of the forbidden region in l–θ space below $l \approx 20$ increases with increasing field strength. If, on the other hand, for some reason the tail of the photon distribution falls off more rapidly than a Wien tail, then the size of the forbidden region above $l \approx 20$ decreases with increasing steepness of the tail. A complete spectral cutoff at $x = \theta$ permits any l for $\theta < 1$.

If confinement does not occur, then the pair-dominated cooling curve (together with $l = l_E$) approximately marks the boundary to a dynamical (denoted above as 'forbidden') region in l–θ space, where steady or non-steady flows of pairs and photons streaming away from the heated plasma region is a consequence of the momentum transfer from photons to pairs. Part of the total luminosity emerges as the energy flux of a pair wind. The prohibitively difficult description of such mildly relativistic flows is not attempted here. The existence of a critical luminosity $l[\theta \approx 1] \approx 20$ (or less if strong enough magnetic fields or external soft photon sources are present) separating static plasma clouds from dynamical ones (pair winds) is likely to have observational consequences. The spectra emerging from pair winds may have qualitatively different features as compared to 'static' spectra either due to radiative transfer effects in the wind or due to the effect of the wind on the surrounding medium.

We find that *for compact sources with $R < 500 R_s$ it is the onset of intensive pair production* (making $l > l_E^{pair}$) *and not $l \approx l_E$ that marks the transition to super-Eddington situations at temperatures* $1/3 < \theta < 3$. For sources of maximum compactness ($R \approx 5R_s$) this transition occurs at $l < l_E$ for $\theta \gtrsim 0.1$ and at $l \approx 0.01 l_E$ for $1/3 < \theta < 3$, i.e. at luminosities considerably smaller than what is normally assumed in the accretion disc literature, where a self-consistent inclusion of pair effects is still to be made.

6 Mildly relativistic plasmas in astronomical objects

Hard X-ray or soft γ-ray emission are signatures of some X-ray binaries, of AGNs, and of γ-ray bursts. In some objects a spectral feature at these photon energies has been interpreted as possibly being an optically thin pair annihilation line (Nolan & Matteson 1983 for Cyg X-1; Bassani & Dean 1983a for NGC 4151 and MCG 8-11-11; Mazets *et al.* 1981 for γ-ray bursts). We give a brief discussion of the few objects observed so far (excluding γ-ray bursts, which are likely to contain strong magnetic fields) with the aim of locating them in l–θ space (Fig. 6).

Although the shortest *detected* time variability at soft X-ray energies in the X-ray binaries Cyg X-1 (Nolan *et al.* 1981) and GX 339-4 (Motch *et al.* 1983) is about 50–80 ms, the true shortest X-ray time-scale is likely to be similar to or shorter than the shortest *detected* optical time-scale, 10–20 ms, in GX 339-4 (Motch, Ilovaisky & Chevalier 1982) and the time, 7.5 ms, the hard X-rays (> 3.5 keV) lag behind the soft X-rays in Cyg X-1 (Page, Bennetts & Ricketts 1981). For Cyg X-1 the low state luminosity is $2 \times 10^{37} (d/2.5\ \mathrm{kpc})^2$ erg s^{-1} (Sunyaev & Trümper 1979; d is the distance) and for a source size $10R_s = 3 \times 10^7$ cm $< R < c\Delta t \approx 3 \times 10^8$ cm with $\Delta t \approx 10$ ms and $M = 10 M_\odot$ we obtain $2 < l < 20$. The relatively soft temperatures ($\theta \lesssim 0.2$) found when fitting the data with unsaturated Comptonization spectra (Sunyaev & Trümper 1979; Nolan & Matteson 1983) together with the moderate value of $l(< 20)$ indicates that the plasma in this object is not pair dominated (i.e. it is below the pair-dominated luminosity curve in Fig. 6). The same holds true for the high energy component ($\theta \approx 1/3$ but l smaller by a factor 10) found by

Nolan & Matteson (1983). Future detected X-ray time variability of less than 20 ms (implying $l > 1$) would rule out the optically thin bremsstrahlung interpretation of Mészaros (1983). The break energy ($\approx\theta > 0.2$) and therefore the total luminosity of GX 339-4 is not yet determined (Nolan *et al.* 1982). The luminosities of these two objects may conflict with the steady luminosity limits imposed by pair balance when an equipartition magnetic field is present.

The observational data of AGNs at γ-ray energies is summarized in Bassani & Dean (1983b). An MeV-hump is observed in the two Seyfert galaxies NGC 4151 (Perotti *et al.* 1979, 1981b) and MCG 8-11-11 (Perotti *et al.* 1981a) with γ-ray luminosities of up to $L(0.5-5\ \mathrm{MeV}) = 2\times10^{45}$ and $7\times10^{46}\ \mathrm{erg\ s^{-1}}$, respectively. The minimum variability time-scale of soft X-rays, Δt_X, from NGC 4151 is about 1 day (Tennant & Mushotsky 1983; Lawrence 1980). If Δt_X is representative for the variability time-scale, Δt_γ, of the MeV-emission, then taking $R \approx c\Delta t_X$ gives $l \approx 20$. For θ in the MeV range this value of l just coincides with the plateau of the pair-dominated luminosity curve in Fig. 6. The shortest detected Δt_X in MCG 8-11-11 is about one month (Ward *et al.* 1977), which gives $l \approx 24$ using the same assumptions as above. The soft γ-ray emission in NGC 4151 and MCG 8-11-11 is therefore consistent (if $\Delta t_\gamma \approx \Delta t_X$) with a steady, pair-dominated plasma having a moderately Comptonized Wien peak. The presence of an equipartition magnetic field is expected to limit the temperature in steady plasmas at $l \approx 20$ to θ smaller than unity, thus necessitating non-steady conditions (pair winds?) in these objects.

Interpreting the MeV-hump in the two galaxies with an optically thin pair annihilation line (Bassani & Dean 1983a) is inconsistent with the assumption of pair balance. The bremsstrahlung emissivity dominates the pair annihilation emissivity at $\theta \gtrsim 3$, while in a steady pair-dominated plasma at $\theta \lesssim 5$ Comptonization, pair annihilation, and photon-photon absorption conspire to produce a Wien peak ($\theta \lesssim 0.4$) or a distorted, somewhat redshifted Wien peak ($0.4 \lesssim \theta \lesssim 5$). *No signature of an optically thin pair annihilation line is expected from plasmas in pair balance.*

Part or all of the soft X-ray emission from NGC 4151 may be the result of repeated flaring occurring at a number of sites throughout the source region (Lawrence 1980). Our idealized uniform cloud is nevertheless expected for large enough l ($\gtrsim 20$) to describe approximately the pair-dominated conditions in between the flaring sites. In particular, the limits imposed by $l_{WE}(\theta)$ should remain valid.

A time variability Δt of about 1 day seems to be emerging as a time-scale of special significance in AGNs. It forms a distinct lower envelope almost independent of the luminosity over 6 orders of magnitude for 2/3 of the objects plotted in a Δt–L diagram by Bassani, Dean & Sembay (1983). Tennant & Mushotzky (1983) found that only one out of 38 AGNs had X-ray variability on time-scales shorter than 3 hr. Similarly, in a study of 51 QSOs Zamorani *et al.* (1984) found X-ray variability to be common on time-scales of 1 day or more, but not on shorter time-scales. The size of the source region is then $R \approx (0.1-1)c\Delta t = (0.3-3)\times10^{15}$ cm and the luminosity L_{pp} characterizing the onset of pair production at mildly relativistic temperatures ($l \approx 20$ at $\theta \approx 1$) becomes $L_{pp} \approx (2-20)\times10^{44}\ \mathrm{erg\ s^{-1}}$ (or less if magnetic fields and soft photon sources are present). Reichert *et al.* (1983) found in a study of 27 AGNs that for $L(2-10\ \mathrm{keV}) > 10^{44}\ \mathrm{erg\ s^{-1}}$ *no* object showed intrinsic absorption, while at $L(2-10\ \mathrm{keV}) < 3\times10^{43}\ \mathrm{erg\ s^{-1}}$ the X-ray source could with equal probability either be uncovered, partially covered or mostly covered by absorbing matter. If the power-law spectrum (energy index ≈ 0.7) extends to 511 keV, then the corresponding luminosity is $(2-7)\times10^{44}\ \mathrm{erg\ s^{-1}}$, similar to the estimate of L_{pp} made above. It could be that pair winds cause the lack of absorption at $L > L_{pp}$ by dispersing the absorbing matter. It is, however, not known what fraction of AGNs have

spectra extending to a few hundred keV. The spectral turnover energy in most QSOs is expected from constraints set by the diffuse X-ray background (Rothschild *et al.* 1983) to occur at $\theta \lesssim 0.2$. This coincides approximately with the maximum allowed temperature in a steady, pair-free plasma cloud radiating at its Eddington limit [$l_E \approx 10^4 (R_s/R) \approx 10^3$, see Section 5 and Fig. 6].

The weak point of the discussion above is the assumption that $\Delta t_\gamma \approx \Delta t_X$. Only after detailed observations of spectral shape *and* time variability in the MeV-range will we be able to make definite statements about the existence of pair plasmas in AGNs.

7 Discussion

We have attempted using the simplest possible means to explore the consequences of imposing pair balance in a mildly relativistic, confined, thermal plasma cloud. In between the previously treated extreme cases of optically thin plasmas and of plasmas in thermodynamic equilibrium there exists a regime with plasmas in Wien equilibrium. The complicated interplay between photon and pair processes in such plasmas was elucidated. The main result was the existence of a pair-dominated luminosity curve that separates a pair-free region from a forbidden one in l–θ space (Fig. 6). Forbidden combinations of l and θ may, however, be allowed if some of our assumptions (in particular that of confinement) are relaxed. Requiring pair balance limits allowed luminosities at mildly relativistic temperatures to values two orders of magnitude smaller than the Eddington luminosity normally employed in accretion models.

This initial study of mildly relativistic plasmas was necessarily incomplete in several respects. In particular, the heating mechanism and the initially heated component (protons, pairs or photons) were not specified and the subsequent energy transfer between the components was not treated (except for our approximate description of Comptonization). The distribution function of the pairs should be determined self-consistently (a power law tail, at least at acceleration sites in the plasma, is a likely possibility). Magnetic field effects, especially the cyclo-synchrotron process should be included. Besides determining the detailed radiative transfer (Stepney 1983; Zdziarski 1984a, b) the dynamical consequences of the momentum transfer from photons to pairs need considerations probably necessitating a kinetic, rather than hydrodynamical, treatment of the pairs. Finally, the astrophysical context, whether accretion on to compact objects or explosive energy release near such objects, should be specified and taken into account. Forthcoming work will address some of these problems.

Acknolwedgments

The author thanks A. Zdziarski and C. I. Björnsson for many valuable discussions and A. Zdziarski for disclosing details of his Monte Carlo simulations in advance of publication. He is also grateful to P. Bristow and C. Stoffer for their excellent typing of a difficult and barely readable manuscript. An HP75C supplied sufficient computing power, while ESO provided the stimulating environment in which this research was conducted.

References

Alexanian, M., 1968. *Phys. Rev.*, **165**, 253.
Araki, S. & Lightman, A. P., 1983. *Astrophys. J.*, **269**, 49.
Bassani, L. & Dean, A. J., 1983a. *Astr. Astrophys.*, **122**, 83.
Bassani, L. & Dean, A. J., 1983b. *Space Sci. Rev.*, **35**, 367.

Bassani, L., Dean, A. J. & Sembay, S., 1983. *Astr. Astrophys.*, **125,** 52.
Bisnovatyi-Kogan, G. S., Zel'dovich, Ya. B. & Sunyaev, R. A., 1971. *Soviet Astr. A.J.*, **15,** 17.
Brown, R. W., Mikaelian, K. O. & Gould, R. J., 1973. *Astrophys. Lett.*, **14,** 203.
Chapline, G. & Stevens, J., 1973. *Astrophys. J.*, **184,** 1041.
Chiu, H. Y., 1968. *Stellar Physics,* Blaisdell, London.
Felten, J. E. & Rees, M. J., 1972. *Astr. Astrophys.*, **17,** 226.
Gould, R. J., 1979. *Astrophys. J.*, **230,** 967.
Gould, R. J. & Schréder, G. P., 1967. *Phys. Rev.*, **155,** 1404.
Guilbert, P. W., Fabian, A. C. & Rees, M. J., 1983. *Mon. Not. R. astr. Soc.*, **205,** 593.
Guilbert, P. W., Fabian, A. C. & Ross, R. R., 1982. *Mon. Not. R. astr. Soc.*, **199,** 763.
Haug, E., 1981. *Z. Naturf.*, **36a,** 413.
Illarionov, A. F. & Sunyaev, R. A., 1972. *Soviet Astr. A.J.*, **16,** 45.
Jackson, J. D., 1975. *Classical Electrodynamics,* 2nd edn, Wiley, New York.
Jauch, J. M. & Rohrlich, F., 1976. *The Theory of Photons and Electrons*, 2nd edn, Springer-Verlag, New York.
Kusunose, M. & Takahara, F., 1983. *Prog. theor. Phys.*, **69,** 1443.
Kylafis, N. D. & Lamb, D. Q., 1982. *Astrophys. J. Suppl.*, **48,** 239.
Lamb, D. Q., 1982. In *Gamma Ray Transients and Related Astrophysical Phenomena,* eds Lingenfelter, R. E., Hudson, H. S. & Worrall, D. H., AIP, New York.
Lawrence, A., 1980. *Mon. Not. R. astr. Soc.*, **192,** 83.
Liang, E. P. T., 1979. *Astrophys. J.*, **234,** 1105.
Lightman, A. P., 1981. *Astrophys. J.*, **244,** 392 (L81).
Lightman, A. P., 1982a. *Astrophys. J.*, **253,** 842 (L82).
Lightman, A. P., 1982b. *Space Sci. Rev.*, **33,** 335.
Lightman, A. P. & Band, D. L., 1981. *Astrophys. J.*, **251,** 713.
Mandl, F. & Skyrme, T. H. R., 1952. *Proc. R. Soc. A,* **215,** 497.
Maxon, M. S. & Corman, E. G., 1967. *Phys. Rev.*, **163,** 156.
Mazets, E. P., Golenetskii, S. V., Aptekar', R. L., Gur'yan, Yu. A. & Il'inskii, V. N., 1981. *Nature,* **290,** 378.
Meier, D. L., 1982. *Astrophys. J.*, **256,** 693.
Mészaros, P., 1983. *Astrophys. J.*, **274,** L13.
Motch, C., Ilovaisky, S. A. & Chevalier, C., 1982. *Astr. Astrophys.*, **109,** L1.
Motch, C., Ricketts, M. J., Page, C. G., Ilovaisky, S. A. & Chevalier, C., 1983. *Astr. Astrophys.*, **119,** 171.
Nolan, P. L., Gruber, D. E., Knight, F. K., Matteson, J. L., Peterson, L. E., Levine, A. M., Lewin, W. H. G. & Primini, F. A., 1982. *Astrophys. J.*, **262,** 727.
Nolan, P. L., Gruber, D. E., Matteson, J. L., Peterson, L. E., Rothschild, R. E., Doty, J. P., Levine, A. M., Lewin, W. H. G. & Primini, F. A., 1981. *Astrophys. J.*, **246,** 494.
Nolan, P. L. & Matteson, J. L., 1983. *Astrophys. J.*, **265,** 389.
Ore, A. & Powell, J. L., 1949. *Phys. Rev.*, **75,** 1696.
Page, C. G., Bennetts, A. J. & Ricketts, M. J., 1981. *Space Sci. Rev.*, **30,** 369.
Perotti, F., Della Ventura, A., Sechi, G., Villa, G., Di Cocco, G., Baker, R. E., Butler, R. C., Dean, A. J., Martin, S. J. & Ramsden, D., 1979. *Nature,* **282,** 484.
Perotti, F., Della Ventura, A., Villa, G., Di Cocco, G., Butler, R. C., Carter, J. N. & Dean, A. J., 1981a. *Nature,* **292,** 133.
Perotti, F., Della Ventura, A., Villa, G., Di Cocco, G., Bassani, L., Butler, R. C., Carter, J. N. & Dean, A. J., 1981b. *Astrophys. J.*, **247,** L63.
Quigg, C., 1968. *Astrophys. J.*, **151,** 1187.
Ramaty, R., McKinley, J. M. & Jones, F. C., 1982. *Astrophys. J.*, **256,** 238.
Rees, M. J., 1981. In *Plasma Astrophysics*, p. 297, eds Guyenne, T. D. & Lévy, G., ESA SP-161, European Space Agency, Paris.
Reichert, G. A., Petre, R., Mushotsky, R. F. & Holt, S. S., 1983. *Bull. Am. Astr. Soc.*, **15,** 675.
Rothschild, R. E., Mushotzky, R. F., Baity, W. A., Gruber, D. E., Matteson, J. L. & Peterson, L. E., 1983. *Astrophys. J.*, **269,** 423.
Rybicki, G. B. & Lightman, A. P., 1979. *Radiative Processes in Astrophysics,* Wiley, New York.
Stepney, S., 1983. In *Positron-Electron Pairs in Astrophysics,* p. 373, eds Burns, M. L., Harding, A. K. & Ramaty, R., AIP, New York.
Stepney, S. & Guilbert, P. W., 1983. *Mon. Not. R. astr. Soc.*, **204,** 1269.
Stoeger, W. R., 1977. *Astr. Astrophys.*, **61,** 659.
Sunyaev, R. A. & Titarchuk, L. G., 1980. *Astr. Astrophys.*, **86,** 121.

Sunyaev, R. A. & Trümper, J., 1979. *Nature,* **279,** 506.
Svensson, R., 1982. *Astrophys. J.,* **258,** 335 (S82).
Svensson, R., 1983. *Astrophys. J.,* **270,** 300.
Tennant, A. F. & Mushotzky, R. F., 1983. *Astrophys. J.,* **264,** 92.
Thorne, K. S., 1981. *Mon. Not. R. astr. Soc.,* **194,** 439.
Wandel, A. & Yahil, A., 1979. *Astr. Astrophys.,* **72,** 367.
Ward, J., Wilson, A. S., Disney, M. J., Elvis, M. & Maccacaro, T., 1977. *Astr. Astrophys.,* **59,** L19.
Weaver, T. A., 1976. *Phys. Rev.,* **A13,** 1563.
Yahel, R. Z., 1982. *Astrophys. J.,* **252,** 356.
Zamorani, G., Giommi, P., Maccacaro, T. & Tananbaum, H., 1984. *Astrophys. J.,* **278,** 28.
Zdziarski, A., 1984a. *Phys. Scripta,* **T7,** 124.
Zdziarski, A., 1984b. *Astrophys. J.,* in press.

Appendix A: soft photon production

All processes of order α^3 with infrared divergences are considered.

A.1 BREMSSTRAHLUNG ($ep \rightarrow ep\gamma$, $ee \rightarrow ee\gamma$)

Useful approximate expressions for the spectral emissivity in the mildly relativistic temperature regime ($\theta \approx 1$) at soft photon energies $x \ll \min[1, \theta]$ are constructed by combining the results obtained at non-relativistic ($\theta \ll 1$) and relativistic temperatures ($\theta \gg 1$) in such a way that the resulting expression reduces to the non-relativistic and relativistic expressions in respective limits.

From the expressions at $\theta \lesssim 1$ given by Kylafis & Lamb (1982) and at $\theta \gg 1$ by Quigg (1968) we obtain for ep-bremsstrahlung

$$\dot{n}_{ep}(x)\,dx = (n_+ + n_-)\, n_p c r_e^2 \alpha \frac{dx}{x} \frac{16}{3} \ln\left[4\eta(1 + C_1\theta)\frac{\theta}{x}\right](1 + 2\theta + 2\theta^2)\,[\exp(1/\theta)K_2(1/\theta)]^{-1}, \tag{A1}$$

where $C_1 = \eta \exp(5/2)/2 \approx 3.42$ and $\eta = \exp(-\gamma_E)$, $\gamma_E \approx 0.5772$ being Euler's number. An exact numerical evaluation of the spectrum shows that the deviations are at most 5 per cent for $x < 0.1\,\theta$ at mildly relativistic temperatures.

Similarly, using the results for soft $e^{\pm}e^{\pm}$-bremsstrahlung at $\theta \ll 1$ (Maxon & Corman 1967) and at $\theta \gg 1$ (Alexanian 1968) gives

$$\dot{n}_{ee}(x)\,dx = (n_+^2 + n_-^2)\, c r_e^2 \alpha \frac{dx}{x} \frac{16}{3} \ln\left[4\eta(C_2 + C_3\theta^2)\frac{\theta}{x}\right]\left(\frac{3}{5}\sqrt{2\theta} + 2\theta^2\right)[\exp(1/\theta)K_2(1/\theta)]^{-1}, \tag{A2}$$

where $C_2 = \exp(29/12) \approx 11.2$ and $C_3 = \eta^2 \exp(7/2) \approx 10.4$. The deviation from the exact numerical results of Stepney & Guilbert (1983) is at most 20 per cent at their smallest photon energy $x = 0.05\theta$ and is likely to be less at softer photon energies.

The e^+e^--bremsstrahlung spectrum is a factor $2^{3/2}$ larger than the ep-spectrum at non-relativistic temperatures, while it is 2 times larger than the $e^{\pm}e^{\pm}$-spectrum at relativistic temperatures (S82). We obtain

$$\dot{n}_{+-}(x)\,dx = n_+ n_- c r_e^2 \alpha \frac{dx}{x} \frac{16}{3} \ln\left[4\eta(1 + C_3\theta^2)\frac{\theta}{x}\right] 2(\sqrt{2} + 2\theta + 2\theta^2)[\exp(1/\theta)\,K_2(1/\theta)]^{-1}, \tag{A3}$$

where the term 2θ in the second to last factor was chosen *ad hoc* to conform to the corresponding term in equation (A1).

The emissivities in equations (A1)–(A3) are shown in Fig. 1 by the curves labelled ep, ee, and +−, respectively.

A.2 DOUBLE COMPTON SCATTERING ($e\gamma \rightarrow e\gamma\gamma$)

The differential cross-section for the double Compton process in an *arbitrary* frame in the soft photon limit ($x \ll \min[1, x_r]$, where x_r is the incoming photon energy in the particle *rest* frame) is given by

$$\frac{d\sigma}{dx}(x, x_r) = \frac{1}{x}\int_{x_r/(1+2x_r)}^{x_r} dx_1 \frac{d\sigma_{cs}}{dx_1}(x_r, x_1)\frac{\alpha}{\pi}\left(\frac{1}{\beta}\ln\frac{1+\beta}{1-\beta} - 2\right), \tag{A4}$$

where $d\sigma_{cs}/dx_1$ is the Compton scattering differential cross-section (Jauch & Rohrlich 1976), x_1 is the outgoing photon energy in the particle *rest* frame, $\beta = (\gamma^2 - 1)^{1/2}/\gamma$ and $\gamma = 1 + x_r - x_1$. The last factor of the integrand comes from the classical photon emission probability for a charged particle accelerating from rest to a final velocity β (Jackson 1975). In deriving equation (A4) use has been made of the Lorentz invariance of dx/x. The following expressions,

$$\frac{d\sigma}{dx}(x, x_r) = \frac{1}{x}\alpha r_e^2 \frac{32}{9}x_r^2 \times (1 + 4.393x_r + 2.064x_r^2 + 9.724\times 10^{-2}x_r^3 - 9.541\times 10^{-4}x_r^4 + 7.757\times 10^{-6}x_r^5)^{-1} \qquad (\log x_r \leqslant 1.6) \tag{A5}$$

and

$$\frac{d\sigma}{dx}(x, x_r) = \frac{1}{x}\alpha r_e^2 \frac{2}{x_r}\left(\ln^2 2x_r - \frac{1}{2}\ln 2x_r - \frac{\pi^2}{6} - \frac{5}{4}\right) \qquad (\log x_r \geqslant 1.6) \tag{A6}$$

are based on the asymptotic ones (the non-relativistic limit was obtained by Gould 1979) and have errors of less than 1.3 per cent.

Using the relativistic rate formalism of Weaver (1976), the double Compton spectral emissivity, $\dot{n}_{DC}(x)\,dx\ \mathrm{cm}^{-3}\,\mathrm{s}^{-1}$, from photons with energy distribution $n(y)\,dy\ \mathrm{cm}^{-3}$ interacting with electrons and positrons with Maxwell–Boltzmann distributions of temperature θ is given by

$$\dot{n}_{DC}(x)\,dx = (n_+ + n_-)\,c\,dx\,[2K_2(1/\theta)]^{-1}\int_0^\infty dx_r\, x_r \frac{d\sigma}{dx}(x, x_r) \times \int_0^\infty dy\, y^{-2}\, n(y)\exp\left[-(x_r/y + y/x_r)/2\theta\right] \qquad (x \ll \min[1, \theta]). \tag{A7}$$

For a photon distribution

$$n(y)\,dy = N_\gamma \tfrac{1}{2}(y/\theta)^q \exp(-y/\theta)\,dy/\theta, \tag{A8}$$

where N_γ is a normalization factor (N_γ is precisely the total photon density, n_γ, when $q = 2$), the spectral emissivity becomes

$$\dot{n}_{DC}(x)\,dx = (n_+ + n_-)\,N_\gamma\,c\,dx\,[2\theta^{1+q}K_2(1/\theta)]^{-1} \times \int_0^\infty dx_r \frac{d\sigma}{dx}(x, x_r)\, x_r^q (1 + 2x_r)^{(1-q)/2} K_{q-1}[(1 + 2x_r)^{1/2}/\theta] \qquad (x \ll \min[1, \theta]). \tag{A9}$$

For a Wien distribution ($q = 2$) the emissivity at $\theta \leqslant 1$ is given by

$$\dot{n}_{DC}(x)\,dx = (n_+ + n_-)\,n_\gamma\,cr_e^2\alpha\,\frac{dx}{x}\,\frac{128}{3}\,\theta^2 g_{DC}(\theta) \qquad (\theta \leqslant 1), \tag{A10}$$

with

$$g_{DC}(\theta) = (1 + 13.91\theta + 11.05\theta^2 + 19.92\theta^3)^{-1}, \tag{A10a}$$

where the latter factor is a fit (error < 3 per cent) to a numerical evaluation of equation (A9). The emissivity, shown in Fig. 1 by the curve labelled DCW, increases as θ^2 at small temperatures, reaches a maximum at $\theta \approx 1$ and decreases at relativistic temperatures roughly as θ^{-2}:

$$\dot{n}_{DC}(x)\,dx = (n_+ + n_-)\,n_\gamma\,cr_e^2\alpha\,\frac{dx}{x}\,\frac{1}{\theta^2}\left(2\ln^2 2\eta\theta + \frac{3}{2}\ln 2\eta\theta + \frac{\pi^2}{12} - \frac{7}{8}\right) \qquad (\theta \gg 1). \tag{A11}$$

L81 and Thorne (1981) obtained equation (A10) in the $\theta \ll 1$ limit, and Lightman & Band (1981) calculated the first term in equation (A11) (obtaining a different logarithmic argument).

The double Compton emissivity for a double Compton-like photon distribution ($q = -1$) is shown in Fig. 1 by the curve labelled DCDC. Here the emissivity does not decrease at relativistic temperatures mainly because the abundance of soft photons offsets the Klein–Nishina decline and the dominating interactions occur at $x_r \approx 1$ (or $y \approx \theta^{-1}$). At non-relativistic temperatures the emissivity becomes

$$\dot{n}_{DC}(x)\,dx = (n_+ + n_-)\,N_\gamma\,cr_e^2\alpha\,\frac{dx}{x}\,\frac{16}{9}\,\theta^2 \qquad (\theta \ll 1), \tag{A12}$$

while at relativistic temperatures the emissivity becomes independent of the temperature

$$\dot{n}_{DC}(x)\,dx = (n_+ + n_-)\,N_\gamma\,c\,dx\,\frac{1}{2}\int_0^\infty dx_r\,\frac{1}{x_r}\,\frac{d\sigma}{dx}(x, x_r)$$

$$= (n_+ + n_-)\,N_\gamma\,cr_e^2\alpha\,\frac{dx}{x}\,2.42 \qquad (\theta \gg 1). \tag{A13}$$

For steeper spectra the emissivity increases monotonically with temperature.

A.3 THREE QUANTUM ANNIHILATION ($e^+e^- \to \gamma\gamma\gamma$)

Using the classical photon emission probability for two particles of equal but opposite charges of energy γ_{cm} coming to rest in the centre of momentum frame (Jackson 1975), the electron–positron pair annihilation cross-section $\sigma_A(\gamma_{cm})$ (Jauch & Rohrlich 1976), and the Lorentz invariance of dx/x the differential cross-section for three quantum annihilation in an *arbitrary* frame in the soft photon limit can be shown to be

$$\frac{d\sigma}{dx}(x, \gamma_{cm}) = \frac{1}{x}\,\frac{\alpha}{\pi}\left(\frac{1+\beta_{cm}^2}{\beta_{cm}}\ln\frac{1+\beta_{cm}}{1-\beta_{cm}} - 2\right)\sigma_A(\gamma_{cm}). \tag{A14}$$

The non-relativistic and relativistic limits are

$$\frac{d\sigma}{dx}(x, \gamma_{cm}) = \frac{1}{x}\,\alpha r_e^2\,\frac{4}{3}\,\beta_{cm}\left(1 + \frac{7}{5}\beta_{cm}^2 \ldots\right) \qquad (\beta_{cm} \ll 1), \tag{A15}$$

and

$$\frac{d\sigma}{dx}(x, \gamma_{cm}) = \frac{1}{x}\,\alpha r_e^2\,\frac{4}{\gamma_{cm}^2}\left(\ln^2 2\gamma_{cm} - \ln 2\gamma_{cm} + \frac{1}{4}\right) \qquad (\gamma_{cm} \gg 1), \tag{A16}$$

respectively. Though a semi-classical description has been used here as well as for double Compton scattering the same results are obtained using relativistic quantum mechanics. The matrix element calculated by Mandl & Skyrme (1952) for double Compton scattering can be applied to three quantum annihilation using the appropriate substitution rules. In the soft photon limit one again obtains equation (A14).

Ore & Powell (1949) calculated the spectral emissivity from three quantum annihilations at *rest*. In that case there is, of course, no infrared divergence, as classically no deceleration occurs before annihilation. In the general case of moving annihilating pairs the spectral emissivity is characterized by a double Compton-like spectrum plus an annihilation peak.

The three quantum annihilation spectral emissivity, $\dot{n}_{3\mathrm{QA}}(x)dx$ cm^{-3} s^{-1}, from thermal pairs of temperature θ in the soft limit becomes

$$\dot{n}_{3\mathrm{QA}}(x)\,dx = n_+ n_-\, c\,dx\, 4\,\theta^{-1}\,[K_2(1/\theta)]^{-2} \times \int_1^\infty d\gamma_{\mathrm{cm}}\,\gamma_{\mathrm{cm}}^4\, 2\beta_{\mathrm{cm}}^2\,\frac{d\sigma}{dx}(x,\gamma_{\mathrm{cm}})\,K_1(2\gamma_{\mathrm{cm}}/\theta) \qquad (x \ll \min[1,\theta]). \tag{A17}$$

At non-relativistic temperatures

$$\dot{n}_{3\mathrm{QA}}(x)\,dx = n_+ n_-\, cr_{\mathrm{e}}^2\,\alpha\,\frac{dx}{x}\,4\theta \qquad (\theta \ll 1), \tag{A18}$$

while at relativistic temperatures

$$\dot{n}_{3\mathrm{QA}}(x)\,dx = n_+ n_-\, cr_{\mathrm{e}}^2\,\alpha\,\frac{dx}{x}\,\frac{1}{\theta^2}\left(2\ln^2 2\eta\theta + \frac{\pi^2}{6} - \frac{1}{2}\right) \qquad (\theta \gg 1). \tag{A19}$$

The behaviour of $\dot{n}_{3\mathrm{QA}}(x)$ at mildly relativistic temperatures is shown in Fig. 1 by the curve labelled 3QA.

A.4 RADIATIVE PAIR PRODUCTION ($\gamma\gamma \rightarrow e^+e^-\gamma$)

Radiative pair production can classically be thought of as two oppositely charged particles created at rest and accelerated to a final energy γ_{cm} in the centre of momentum frame. The differential cross-section is given by equation (A14) of the annihilation cross-section is replaced by the photon–photon pair production cross-section. To obtain the spectral emissivity, $\dot{n}_{\mathrm{RPP}}(x)dx$ cm^{-3} s^{-1}, from radiative pair productions by photons with Wien distributions one can simply use the detailed balance relations between the pair annihilation and the photon–photon pair production processes (Svensson 1983), giving

$$\dot{n}_{\mathrm{RPP}}(x)\,dx = \frac{n_\gamma^2}{n_+ n_-}\left[\frac{K_2(1/\theta)}{2\theta^2}\right]^2 \dot{n}_{3\mathrm{QA}}(x)\,dx. \tag{A20}$$

If the plasma is in Wien equilibrium, then $\dot{n}_{\mathrm{RPP}}(x) = \dot{n}_{3\mathrm{QA}}(x)$ (using equation 2.8), as can be seen in Fig. 1.

A.5 TOTAL PHOTON PRODUCTION RATE

The total production rate, $\dot{n}_\gamma$ cm^{-3} s^{-1}, of photons with energies larger than x_{m} is given by

$$\dot{n}_\gamma = \int_{x_{\mathrm{m}}}^\infty dx\,\dot{n}(x). \tag{A21}$$

The spectral emissivities $\dot{n}(x)$ decrease exponentially at photon energies above $x = \theta$. We will approximate $\dot{n}(x)$ in the energy range $x_m < x < \theta$ with the soft rates obtained above and with a sharp cutoff at $x = \theta$. The soft bremsstrahlung rates are of the form $x^{-1} \ln(A\theta/x)$ (A depends on temperature only), while the other rates are of the form x^{-1}. Evaluating the integrals gives

$$\int_{x_m}^{\theta} dx\, x^{-1} \ln(A\theta/x) = \ln(\theta/x_m) \ln(A\sqrt{\theta/x_m}) \tag{A22a}$$

and

$$\int_{x_m}^{\theta} dx\, x^{-1} = \ln(\theta/x_m). \tag{A22b}$$

A.6 THE ABSORPTION COEFFICIENTS

The total absorption coefficient, $a_{abs}(x)\ \mathrm{cm}^{-1}$, is the sum of the absorption coefficients for the separate processes (bremsstrahlung and double Compton in this paper). Using Kirchhoff's law gives

$$a_{abs}(x) = \sum_i a_i(x) = \frac{\sum_i \dot{n}_i(x)}{c\, n_{BB}(x)}, \tag{A23}$$

where $n_{BB}(x)\,dx\ \mathrm{cm}^{-3}$ is the 'black body' photon density in an energy interval dx,

$$n_{BB}(x) = \lambda\!\!\!^{-3} \pi^{-2} x^2 [\exp(x/\theta) - 1]^{-1}. \tag{A24}$$

For $x \ll \theta$ the absorption coefficient becomes

$$a_{abs}(x) = \frac{\lambda\!\!\!^{3}}{c} \pi^2 (x\theta)^{-1} [\dot{n}_{ep}(x) + \dot{n}_{ee}(x) + \dot{n}_{+-}(x) + \dot{n}_{DC}(x)]. \tag{A25}$$

Appendix B: two body reaction rates in Wien equilibrium plasmas

B.1 PHOTON–PHOTON PAIR PRODUCTION ($\gamma\gamma \rightarrow e^+e^-$)

The photon–photon pair production rate, $(\dot{n}_+)_{\gamma\gamma}\ \mathrm{cm}^{-3}\ \mathrm{s}^{-1}$, from two photon distributions of power law shapes with exponential high energy cutoffs (described by equation A8 with normalization factors N_i, power law slopes q_i, and cutoff energies θ_i, $i = 1, 2$, respectively) is given by

$$(\dot{n}_+)_{\gamma\gamma} = \frac{N_1 N_2}{1 + \delta_{12}} c r_e^2 \frac{1}{2} \pi \theta_1^{-1-q_1} \theta_2^{-1-q_2} \left(\frac{\theta_1}{\theta_2}\right)^{(q_1 - q_2)/2}$$

$$\times \int_1^{\infty} ds_0\, \phi(s_0)\, s_0^{(q_1+q_2-4)/2} K_{q_1-q_2}[2(s_0/\theta_1\theta_2)^{1/2}], \tag{B1}$$

where $\phi(s_0)$ is a function ($\propto$ the angle averaged cross-section) given by Gould & Schréder (1967; for corrections see Brown, Mikaelian & Gould 1973), and δ_{12} is the Kronecker delta.

For non-relativistic 'cut-off' energies ($\theta_1, \theta_2 \ll 1$) the production rate becomes

$$(\dot{n}_+)_{\gamma\gamma} = \frac{N_1 N_2}{1+\delta_{12}} cr_e^2 \frac{1}{4} \pi^2 \theta_1^{1/2-q_1} \theta_2^{1/2-q_2} \left(\frac{\theta_1}{\theta_2}\right)^{(q_1-q_2)/2} \exp\left[-2/(\theta_1\theta_2)^{1/2}\right]. \tag{B2}$$

Two special cases of equation (B1) are of interest in this paper. First, consider pair production when both photons belong to the same Wien distribution. In this case $\delta_{12} = 1$, $\theta_1 = \theta_2 = \theta$, $q_1 = q_2 = 2$, and $N_1 = N_2 = n_\gamma$, where n_γ is the photon density and equation (B1) simplifies into

$$(\dot{n}_+)_{\gamma\gamma} = n_\gamma^2 cr_e^2 \frac{1}{4} \pi \theta^{-6} \int_1^\infty ds_0 \phi(s_0) K_0(2s_0^{1/2}/\theta). \tag{B3}$$

For Wien distributions it is also possible to write the production rate as an integral over the photon–photon pair production cross-section, $\sigma_{\gamma\gamma}$ (Jauch & Rohrlich 1976), using the results of Weaver (1976),

$$(\dot{n}_+)_{\gamma\gamma} = n_\gamma^2 c \theta^{-5} \int_1^\infty dx_{cm} x_{cm}^4 \sigma_{\gamma\gamma}(x_{cm}) K_1(2x_{cm}/\theta), \tag{B4}$$

where x_{cm} is the photon energy in the centre of momentum frame. Equation (B4) is intimately connected with the expressions (equations 23 and 24 in Svensson 1983) for the thermal pair annihilation rate, $\dot{n}_A$ cm^{-3} s^{-1}, as is demanded by detailed balance. The ratio between the two rates simply becomes

$$\frac{(\dot{n}_+)_{\gamma\gamma}}{\dot{n}_A} = \frac{n_\gamma^2}{n_+ n_-} \left[\frac{K_2(1/\theta)}{2\theta^2}\right]^2, \tag{B5}$$

which is unity in Wien equilibrium (using equation 2.8).

The behaviour of $(\dot{n}_+)_{\gamma\gamma}$ for Wien distributions is shown in fig. 2 in Weaver (1976), where the non-relativistic result is also given. The following expressions based on the asymptotic ones,

$$(\dot{n}_+)_{\gamma\gamma} = n_\gamma^2 cr_e^2 \frac{1}{8} \pi^2 \theta^{-3} \exp(-2/\theta)(1 + 2.88\theta^{0.934}) \qquad (\theta < 1) \tag{B6a}$$

and

$$(\dot{n}_+)_{\gamma\gamma} = n_\gamma^2 cr_e^2 \frac{1}{2} \pi \theta^{-2} \ln(2\eta\theta + 0.38) \qquad (\theta > 1) \tag{B6b}$$

have a maximum error of 2 per cent.

Secondly, we are interested in the case $q_1 = -1$, $q_2 = 2$, i.e. a Wien distribution interacting with the 'flat' part of a fully Comptonized photon distribution in a bremsstrahlung-dominated plasma. Here $\theta_1 = \theta_2 = \theta$, $N_2 = n_\gamma$, $\delta_{12} = 0$ and the pair production rate is written as

$$(\dot{n}_+)_{\gamma\gamma} = N_1 n_\gamma cr_e^2 \frac{1}{4} \pi^2 \exp(-2/\theta) I(\theta), \tag{B7}$$

where $0.99 < I(\theta) < 1.3$. The function $I(\theta)$ becomes 1 for $\theta \ll 1$, while in the relativistic limit

$$I(\theta) = \frac{2}{\pi} \int_1^\infty ds_0 s_0^{-3} \phi(s_0) = \frac{2}{\pi^2} \int_1^\infty dx_{cm} x_{cm}^{-1} [\sigma_{\gamma\gamma}(x_{cm})/r_e^2] = \frac{28}{9\pi} \approx 0.99 \qquad (\theta \gg 1). \tag{B8}$$

For our purposes setting $I(\theta) = 1$ at all θ provides sufficient accuracy.

B.2 PHOTON-ELECTRON (OR POSITRON) PAIR PRODUCTION ($\gamma e \rightarrow e e^+ e^-$)

The photon–electron pair production rate, $(\dot{n}_+)_{\gamma e}\ \mathrm{cm^{-3}\ s^{-1}}$, from a photon Wien distribution interacting with a particle Maxwell–Boltzmann distribution of the same temperature is given by

$$(\dot{n}_+)_{\gamma e} = n_\gamma (n_+ + n_-) c \frac{1}{2} \theta^{-4} [K_2(1/\theta)]^{-1} \int_4^\infty dx\, x^2\, \sigma_{\gamma e}(x)\, y^{-1}\, K_1(y), \tag{B9}$$

where $y = (1 + 2x)^{1/2}/\theta$ and x is the photon energy in the particle rest frame. A simple fit to the cross-section $\sigma_{\gamma e}(x)$ is found in Haug (1981). (The factor $3\ \pi^{1/2}$ in equation (31) in S82 should be replaced by $\pi 3^{1/2}$.) Applying correction factors to the asymptotic limits of equation (B9) gives expressions that are accurate to within 6 per cent,

$$(\dot{n}_+)_{\gamma e} = n_\gamma (n_+ + n_-)\, c r_e^2 \alpha \frac{4\pi}{27} \exp(-2/\theta) \times \begin{cases} (1 + 27.1\theta^{0.949}) & (\theta \leqslant 0.18) \quad \text{(B10a)} \\ 16.1\theta^{0.541} & (0.18 \leqslant \theta \leqslant 2) \quad \text{(B10b)} \end{cases}$$

and

$$(\dot{n}_+)_{\gamma e} = n_\gamma (n_+ + n_-)\, c r_e^2 \alpha \left(\frac{56}{9} \ln 2\eta\theta - \frac{8}{27}\right)(1 + 0.5/\theta)^{-1} \qquad (\theta \geqslant 2). \tag{B10c}$$

B.3 PHOTON–PROTON PAIR PRODUCTION ($\gamma p \rightarrow p e^+ e^-$)

The photon–proton pair production rate, $(\dot{n}_+)_{\gamma p}\ \mathrm{cm^{-3}\ s^{-1}}$, is given to 10 per cent accuracy by

$$(\dot{n}_+)_{\gamma p} = n_\gamma n_p\, c r_e^2 \alpha \pi \theta \exp(-2/\theta)(1 + 0.9\theta)^{-1} \qquad (\theta \leqslant 2) \tag{B11a}$$

and

$$(\dot{n}_+)_{\gamma p} = n_\gamma n_p\, c r_e^2 \alpha \left[\frac{28}{9} \ln(2\eta\theta + 1.7) - \frac{92}{27}\right] \qquad (\theta \geqslant 2), \tag{B11b}$$

obtained by applying fitting factors to the asymptotic expressions. The recent fit of the cross-section by Stepney & Guilbert (1983) was used in the calculations. (Equation 40 in S82 should be multiplied by a factor 1/8.)

B.4 COMPTON SCATTERING ($\gamma e \rightarrow \gamma e$)

The Compton scattering rate, $\dot{n}_{cs}\ \mathrm{cm^{-3}\ s^{-1}}$, is (with an appropriate change of integration limits and cross-section) given by equation (B9). A Wien-averaged scattering opacity is defined by

$$a_w(\theta) \equiv \frac{\dot{n}_{cs}}{c n_\gamma} = (n_+ + n_-)\, \sigma_T g_\tau(\theta), \tag{B12}$$

where

$$g_\tau(\theta) = \begin{cases} (1 + 5\theta + 0.4\theta^2)^{-1} & (\theta \leqslant 1) \quad \text{(B13a)} \\ \frac{3}{16} \theta^{-2} \left(\ln 2\eta\theta + \frac{3}{4}\right)(1 + 0.1/\theta)^{-1} & (\theta \geqslant 1), \quad \text{(B13b)} \end{cases}$$

and where the error is less than 4 per cent. The corresponding Wien-averaged scattering optical depth, τ_w, of a region with a Thomson scattering depth τ_T is given by

$$\tau_w = \tau_T g_\tau(\theta). \tag{B14}$$

Appendix C: Mildly relativistic Comptonization

Previous attempts analytically to quantify moderate Comptonization (i.e. all photons do not scatter into the Wien peak before escaping) at non-relativistic temperature were made by Chapline & Stevens (1973) and Meier (1982). Neither work provides suitable results for our purposes. Meier, for example, uses the non-relativistic Compton y-parameter ($\equiv 4\theta\tau_T^2$) as the critical parameter determining whether the Comptonization is saturated ($y > 1$) or not ($y < 1$). However, as Lightman & Band (1981) correctly point out, Comptonization becomes saturated for $y > \ln(\theta/x_{coh})$ (for x_{coh}, see Appendix D), while being moderate for $1 < y < \ln(\theta/x_{coh})$. Non-coherent effects are unimportant for $y < 1$.

Here we choose to quantify moderate Comptonization at non-relativistic as well as mildly relativistic temperatures by determining the *fraction* of photons that scatter into the Wien-peak before escaping.

The number of scatterings $N(x_i, x_f)$ that a photon of initial energy x_i needs to reach a mean final energy x_f is approximately

$$N(x_i, x_f) = \frac{\ln(x_f/x_i)}{\ln(1 + 4\theta + 16\theta^2)}, \tag{C1}$$

which differs by at most 10 per cent from more detailed results (equation 2.6 in Guilbert, Fabian & Ross 1982). Sunyaev & Titarchuk (1980) discuss the normalized probability distribution $P(N)$ for a photon to undergo N scatterings before escaping from a medium having a specified spatial distribution of photon sources. Here we use the simple form (*cf.* equation 9 in Sunyaev & Titarchuk 1980)

$$P(N) = (\xi\tau_T^2)^{-1} \exp[-N/(\xi\tau_T^2)], \tag{C2}$$

where τ_T is the Thomson scattering optical depth of the medium and $0.2 \lesssim \xi \lesssim 1$ is a factor dependent on the geometry and the distribution of photon sources (for quantitative estimates we use $\xi = 1/3$). The fraction $f(x)$ of photons of initial energy $x_i = x$ that will reach final energies larger than θ before escaping is then

$$f(x) = \int_{N(x,\theta)}^{\infty} dN' P(N') = \exp\left[-\frac{\ln(\theta/x)}{\xi\tau_T^2 \ln(1 + 4\theta + 16\theta^2)}\right]. \tag{C3}$$

For photons emitted according to a normalized bremsstrahlung emissivity

$$S_B(x)\,dx = 2\frac{\ln(\theta/x)}{\ln^2(\theta/x_m)}\frac{dx}{x} \qquad (x_m < x < \theta). \tag{C4}$$

the fraction reaching final energies $> \theta$ is simply

$$f_B(y_1) = \int_{x_m}^{\theta} dx\, f(x)\, S_B(x) = 2[y_1^2 - (y_1 + y_1^2)\exp(-1/y_1)], \tag{C5}$$

where

$$y_1 \equiv \xi\frac{\tau_T^2 \ln(1 + 4\theta + 16\theta^2)}{\ln(\theta/x_m)} \tag{C6}$$

is the crucial parameter describing the transition ($f_B = 0.53$ for $y_1 = 1$) between saturated ($y_1 > 1$; $f_B = 1 - 2/(3y_1)$ for $y_1 \gg 1$) and moderate ($y_1 < 1$; $f_B = 2y_1^2$ for $y_1 \ll 1$) Comptonization. The non-relativistic energy amplification factor (used in Fig. 6) becomes

$$A = 1 + f_B(y_1)\frac{3}{4}\ln^2\frac{\theta}{x_m}, \tag{C7}$$

which have the correct limits ($A = 1$ for $y \ll 1$ and $A = (3/4)\ln^2(\theta/x_m)$ for $y_1 \gg 1$).

Similarly, for a normalized double Compton emissivity

$$S_{DC}(x) = \frac{1}{\ln(\theta/x_m)}\frac{dx}{x} \qquad (x_m < x < \theta), \tag{C8}$$

the corresponding fraction becomes

$$f_{DC}(y_1) = \int_{x_m}^{\theta} dx\, f(x)\, S_{DC}(x) = y_1[1 - \exp(-1/y_1)]. \tag{C9}$$

We take f_B and f_{DC} to represent the fraction of bremsstrahlung and double Compton photons that are scattered *into the Wien-peak* before escaping. A few neglected effects at mildly relativistic temperatures should be kept in mind: (1) the shape of $S_B(x)$ differs somewhat from equation (C4); (2) any scattering at $x > \theta^{-1}$ occurs in the decreasing Klein–Nishina limit of the cross-section, which may (3) cause the scattering optical depth at these photon energies to be less than unity (even though $\tau_T > 1$) in which case the spectral shape is not Wien, but rather determined by the kinematics of the last scattering.

Appendix D: determination of x_m

Determining the photon energy, x_m, below which the *local* spectrum is Planckian, requires the introduction of four characteristic photon energies: x_0, x_{abs}, x_t and x_{coh} (*cf.* the notation of Rybicki & Lightman 1979). The energy x_0, at which the time-scales for a photon to get absorbed or to get scattered are equal, is determined by

$$a_{cs}(x_0) = a_{abs}(x_0), \tag{D1a}$$

where $a_{cs}(x_0)\,\mathrm{cm}^{-1}$ and $a_{abs}(x_0)\,\mathrm{cm}^{-1}$ are the Compton scattering coefficient (equation 62 in S82) and the absorption coefficient (equation A25), respectively. At the energy x_{abs} the absorption time-scale is equal to the time-scale for escape from a plasma having a scattering optical depth $\tau_{cs} < 1$. This condition can be written as

$$a_{cs}(x_{abs}) = a_{abs}(x_{abs})\,\tau_{cs}(x_{abs}). \tag{D1b}$$

The corresponding condition in a plasma having $\tau_{cs} > 1$ determines x_t,

$$a_{cs}(x_t) = a_{abs}(x_t)\,\xi\,\tau_{cs}^2(x_t), \tag{D1c}$$

where the factor ξ is discussed in Appendix C. Finally, x_{coh} is the photon energy, where the time-scale for absorption equals the time-scale for a photon to increase its energy due to Compton scatterings. The number of scatterings needed is $(4\theta)^{-1}$ at non-relativistic temperatures and 1 at mildly relativistic temperatures. This is most simply described through

$$a_{cs}(x_{coh}) = a_{abs}(x_{coh})\frac{1}{\min[1, 8\theta]}, \tag{D1d}$$

where following L81 an extra factor of 2 was introduced.

At non-relativistic temperatures (θ less than, say, 1/8) τ_{cs} is equal to the Thomson scattering depth τ_T and x_m is equal to (i) x_{abs} for $\tau_T < 1$, (ii) x_t for $1 < \tau_T < (\xi 8\theta)^{-1/2}$, and (iii) x_{coh} for $\tau_T > (\xi 8\theta)^{-1/2}$. At relativistic temperatures ($\theta > 1/8$) we have (i) $x_m = x_{abs}$ for $\tau_{cs} < 1$, and (ii) $x_m = x_0 = x_{coh}$ for $\tau_{cs} > 1$. In our applications x_m is always in the Thomson limit and $\tau_{cs} = \tau_T$ or $a_{cs} = a_T \equiv (n_+ + n_-)\sigma_T$. We determine x_m by solving

$$a_T = a_{abs}(x_m)\frac{\tau_T(1+\xi\tau_T)}{1+\xi\tau_T^2 \min[1, 8\theta]}, \tag{D2}$$

which reduces to equations (D1a)–(D1d) in the appropriate limits.

For $\tau_T > 1$ a Planckian is achieved in the *emergent* spectrum below x_0 only.